HHS Public Access

Author manuscript

Sci Transl Med. Author manuscript; available in PMC 2023 June 17.

Published in final edited form as:

Sci Transl Med. 2022 October 05; 14(665): eabn2956. doi:10.1126/scitranslmed.abn2956.

Metabolic modulation of synaptic failure and thalamocortical hypersynchronization with preserved consciousness in Glut1 deficiency

Karthik Rajasekaran[1,†,‡], **Qian Ma**[1,†], **Levi B. Good**[1], **Gauri Kathote**[1], **Vikram Jakkamsetti**[1], **Peiying Liu**[2,§], **Adrian Avila**[1], **Sharon Primeaux**[1], **Julio Enciso Alva**[3], **Kia H. Markussen**[4], **Isaac Marin-Valencia**[1,‖], **Deepa Sirsi**[5], **Peter M. S. Hacker**[6,7], **Matthew S. Gentry**[4], **Jianzhong Su**[3], **Hanzhang Lu**[2,§], **Juan M. Pascual**[1,5,8,9,*]

[1]Rare Brain Disorders Program, Department of Neurology, University of Texas Southwestern Medical Center, Dallas, TX 75390, USA.

[2]Advanced Imaging Research Center, University of Texas Southwestern Medical Center, Dallas, TX 75390, USA.

[3]Department of Mathematics, University of Texas at Arlington, Arlington, TX 76019, USA.

[4]Department of Molecular and Cellular Biochemistry, University of Kentucky, Lexington, KY 40506, USA.

[5]Department of Pediatrics, University of Texas Southwestern Medical Center, Dallas, TX 75390, USA.

[6]St. John's College and Department of Philosophy, University of Oxford, Oxford OX1 3JP, UK.

[7]University College London Queen's Square Institute of Neurology, London WC1N 3BG, UK.

[8]Department of Physiology, University of Texas Southwestern Medical Center, Dallas, TX 75390, USA.

[9]Eugene McDermott Center for Human Growth and Development/Center for Human Genetics, University of Texas Southwestern Medical Center, Dallas, TX 75390, USA.

Abstract

[*]Corresponding author. juan.pascual@UTsouthwestern.edu.
[†]These authors contributed equally to this work.
[‡]Present address: Jazz Pharmaceuticals, Palo Alto, CA 94304, USA.
[§]Present address: Department of Radiology and Radiological Science, Johns Hopkins University, Baltimore, MD 21218, USA.
[‖]Present address: Department of Neurology, Mount Sinai School of Medicine, New York, NY 10029, USA.

Author contributions: Conceptualization: J.M.P. Methodology: J.M.P., H.L., J.S., and M.S.G. Investigation: all authors. Funding acquisition: J.M.P. Project administration: J.M.P. Supervision: J.M.P. Writing—original draft: K.R., J.M.P., and P.M.S.H. Writing—review and editing: all authors.

Competing interests: The authors declare that they have no competing interests.

Data and materials availability: The data obtained from neurophysiological studies are in data file S1. Data acquired in mouse PET studies are in data file S2. Mouse MS data are in data file S3. UT Southwestern Medical Center materials transfer agreements apply to the G1D-deficient mice.

SUPPLEMENTARY MATERIALS
www.science.org/doi/10.1126/scitranslmed.abn2956

Individuals with glucose transporter type I deficiency (G1D) habitually experience nutrient-responsive epilepsy associated with decreased brain glucose. However, the mechanistic association between blood glucose concentration and brain excitability in the context of G1D remains to be elucidated. Electroencephalography (EEG) in G1D individuals revealed nutrition time-dependent seizure oscillations often associated with preserved volition despite electrographic generalization and uniform average oscillation duration and periodicity, suggesting increased facilitation of an underlying neural loop circuit. Nonlinear EEG ictal source localization analysis and simultaneous EEG/functional magnetic resonance imaging converged on the thalamus-sensorimotor cortex as one potential circuit, and ^{18}F-deoxyglucose positron emission tomography (^{18}F-DG-PET) illustrated decreased glucose accumulation in this circuit. This pattern, reflected in a decreased thalamic to striatal ^{18}F signal ratio, can aid with the PET imaging diagnosis of the disorder, whereas the absence of noticeable ictal behavioral changes challenges the postulated requirement for normal thalamocortical activity during consciousness. In G1D mice, ^{18}F-DG-PET and mass spectrometry also revealed decreased brain glucose and glycogen, but preserved tricarboxylic acid cycle intermediates, indicating no overall energy metabolism failure. In brain slices from these animals, synaptic inhibition of cortical pyramidal neurons and thalamic relay neurons was decreased, and neuronal disinhibition was mitigated by metabolic sources of carbon; tonic-clonic seizures were also suppressed by α-amino-3-hydroxy-5-methyl-4-isoxazolepropionic acid (AMPA) receptor inhibition. These results pose G1D as a thalamocortical synaptic disinhibition disease associated with increased glucose-dependent neuronal excitability, possibly in relation to reduced glycogen. Together with findings in other metabolic defects, inhibitory neuron dysfunction is emerging as a modulable mechanism of hyperexcitability.

INTRODUCTION

The main biological activities of the brain are modulated by glucose consumption and neuronal excitability. Both aspects are interrelated as may be inferred not only from biochemical principles, given that glucose is the metabolic substrate for the almost ubiquitous neurotransmitter glutamate and γ-aminobutyric acid (GABA), but also from disorder states. Physiologic changes in blood glucose concentration do not affect neural metabolism or excitation due to the robust glucose transport capacity of the brain (1); however, hypoglycemia can lead to cell death through a form of glutamate hyperexcitability termed excitotoxicity. Furthermore, a more moderate degree of brain glucose depletion leads to decreased cerebral electrical activity through reduction of tricarboxylic acid (TCA) cycle–derived amino acids such as glutamate and glutamine (2). These complex effects suggest the contribution of distinct or differentially affected mechanisms at play in each metabolic state. In support of this hypothesis, it has been noted that genetic defects of brain metabolism can lead to paradoxical periodic hyperexcitability or epilepsy associated with moderate metabolic flux reduction (3, 4).

Glucose transporter Glut1 deficiency syndrome (G1D) is caused by haploinsufficiency of the gene *slc2a1* coding for the glucose transporter of red blood, endothelial, and glial cells. Diminished brain glucose flux in the setting of normoglycemia is associated with seizures as part of a broader-ranging G1D encephalopathy (5). These seizures may number in the hundreds daily and can be mitigated by meals in the timeframe expected of a

modulatory effect by increased brain glucose (6). In normal conditions, even relatively large blood glucose concentration changes do not affect the cerebral metabolic rate of normal persons (7). This unusual presumed enhanced metabolic dependence is in fact exploited by therapeutic carbohydrate-rich, specific lipid–rich, or ketogenic diets, which are used primarily to mitigate G1D epilepsy (6, 8, 9). Thus, we set out to identify the mechanism of excitability in G1D by first characterizing the salient aspects of the epilepsy typical of the human disorder and then, informed by this characterization, we used a mouse model to elucidate the mechanism.

RESULTS

Electroencephalographic epileptic oscillations in individuals with G1D

To characterize electroencephalography (EEG) activity, we performed standard clinical 23-hour EEG recordings in 45 G1D individuals not receiving a therapeutic ketogenic diet. In 40 of them, nearly stereotypic, elevated amplitude oscillations were detected by all the recording electrodes. These oscillations consisted of series of repetitive spike-wave discharges of abrupt onset, with each discharge lasting 250 to 500 ms, that reached steady electrical amplitude and lasted for a variable time until gradually disappearing. This activity disrupted the normal electrocerebral background or interictal rhythm in a manner apparently indistinguishable from other so-called idiopathic absence epilepsy seizures. Figure 1 (A and E) illustrates typical oscillations composed of a brief spike followed by a better-defined, larger-amplitude slower wave with a periodicity of 2.0 to 4.0 Hz ($n > 200$ seizures from 40 individuals). In contrast with similar EEG findings typical of absence epilepsy, where the affected person loses consciousness, albeit briefly, during the seizure, G1D discharges often (12 of 23 discharges spanning over 3 s in eight G1D individuals analyzed with simultaneous video-EEG) did not impair the conscious activity that the person manifested as illustrated in movies S1 and S2 for an individual who is answering a question or reciting a number list before and during one such seizure. Individual observations of reduced absence episodes upon meal consumption or after intentional carbohydrate intake [J.M.P.'s clinical observations from $n = 145$ individuals and (10)] led us to study the temporal evolution and morphology of electrographic oscillations after consumption of the nontherapeutic meal habitually preferred by each individual several times during the day (fig. S1). As expected, meals were followed by a significant ($P < 0.05$; Fig. 1C and data file S1) decrease in seizure onset probability. Because there is no known systemic carbohydrate metabolism abnormality in G1D, the temporal evolution of this effect is compatible with increased blood glucose concentration (11). In contrast, in each G1D participant, post-meal seizure duration and oscillation periodicity were not significantly different from pre-meal values ($P > 0.05$, paired t tests for individuals C to H in Fig. 1D and data file S1). This suggests that meals, or elevated blood glucose concentration, decrease seizure likelihood but, once triggered, G1D seizures are stereotypic events. In contrast, the variable oscillation frequency of non-G1D seizures in general and of other spike-wave epilepsies such as that exemplified in Fig. 1B is consistent with the notion that changes in EEG oscillatory frequency may arise from the action of multiple neural circuits or mechanisms (12). Thus, a possible interpretation of the uniformity of G1D EEG discharge oscillation frequency and high likelihood of preservation

of consciousness is stereotypic activation of one circuit rather than a multiplicity of them as may be the case in other epilepsies.

Source localization of human G1D seizures

To estimate the temporal course of EEG signal propagation across brain structures, which can help identify areas of seizure origin, we generated a tridimensional mathematical model of the brain for EEG source localization by correlating 22 potential brain structural electrical sources (11 from the left and 11 from the right hemisphere) with the temporal evolution of seizures subdivided in five 20%-time segments (from seizure start to cessation) in six individuals with G1D. This allowed us to infer the position of the current sources from electrode potentials (13). Because abnormalities of brain configuration occur in 27% of individuals with G1D as noted by standard clinical magnetic resonance imaging (MRI) (9), we visually examined MRIs to ensure absence of deviation from normal at clinical MRI resolution level. G1D is also associated with microcephaly in some individuals. Thus, normocephalic individuals were selected. Furthermore, head circumference measurements were used to estimate brain volume as guided by normative autopsy correlative data obtained in normal individuals in relation to their head circumference (14), and the circumference range obtained from these measurements yielded a variability of <10% in brain volume, which exerted a negligible influence on the source calculations. To further mitigate any unapparent individual brain inhomogeneities, the source localization model incorporated relatively large, anatomically distinct brain regions such as those typically discernible in functional MRI (fMRI) studies of averaged groups of individuals. Figure 2 and fig. S2 to S4 (data file S1) illustrate the inferred participation of each brain structure as seizures progress from onset to extinction, in addition to the effect of subdividing the cortex into regions on the source estimates. The distribution of the EEG signal was dependent on brain region and time into the seizure. Among several structures identified at seizure onset (0 to 20% of the seizure interval; Fig. 2) were the sensorimotor cortex and the thalamus. Activity in premotor and somatosensory cortices preceded that in other regions, including parieto-occipital, visual, and temporal cortices and thalamus in the early seizure time segments ($P < 0.05$). The precedence of premotor and somatosensory cortices over frontal cortex was not significant ($0.05 < P < 0.06$). Further subdivision of this cortical area into somatosensory, motor, and additional cortical subdivisions (fig. S3 and S4) yielded similar results. Figure S4 complementarily illustrates derivative source localization estimates for nucleus accumbens, amygdala, caudate nucleus, cerebral cortex, cerebral white matter, hippocampus, lateral ventricle, pallidum, putamen, thalamus, and ventral diencephalon. Movie S3 illustrates the evolution of the estimated source across the brain as one seizure progresses in one individual.

Thalamocortical activity during G1D seizures

To further delineate brain regions where changes in neural activity are synchronized with the seizure discharge, we used metabolic imaging. To this end, we performed simultaneous EEG-fMRI recordings in six adult individuals with G1D who were able to remain awake and experienced frequent seizures of sufficient duration for adequate resolution of the blood oxygen level–dependent (BOLD) signal. One limitation of this method is that it complements the signal source localization results above with greater spatial accuracy

but at the expense of lower temporal resolution. Another limitation is its applicability primarily to awake adults, because children generally cannot comply with the rigors of MRI scanning and anesthesia would likely interfere with seizures. Considering all the studied G1D individuals, average cumulative seizure duration was 16 ± 8% of the total EEG recording time inside the MRI scanner (Fig. 3, A and C). During these seizures, BOLD signal increased in the cortical sensorimotor cortex and thalamus in addition to other frontal, visual, and auditory cortices and subcortical and cerebellar areas (Fig. 3), whereas BOLD decreased in the cingulate gyrus and basal ganglia (fig. S5), which is reminiscent of other types of absence seizures of unknown cause (15). In those epilepsies, BOLD-fMRI increases in the cortex and thalamus during spike-wave discharges are associated with increased neuronal excitability in these regions (16), suggesting by analogy that this is also the case in G1D.

Regional human brain glucose deficiency in G1D at rest

We next evaluated regions identified by source localization and BOLD activation during or at the onset of seizures for glucose accumulation at rest, when the awake G1D participants were not engaged in a directed task, via ^{18}F-deoxyglucose positron emission tomography (^{18}F-DG-PET) (Fig. 4). Contrary to a widespread notion, the ^{18}F signal arises from accumulation (influx minus efflux) of the radioactive label rather than from glucose uptake. Individual molecular Glut1 activity amounts to about 50 to 90% of normal but is not absent as the result of most pathogenic haploinsufficiency mutations (17). This reduced activity is compounded across a series of consecutive Glut1-containing cellular barriers to glucose flux. Thus, despite uncertainty about the number of such barriers and the degree of glucose retention or modification due to metabolism inside each cell type, we expected a decrease in labeled brain glucose signal before metabolic steady state was reached by the ^{18}F-DG tracer in the brain. Decreased relative ^{18}F signal is used in epileptology to identify seizure foci. We previously demonstrated a regional pattern of qualitatively decreased glucose-related signal in G1D individuals at rest (^{18}F-DG tracer distribution time was 30 min and PET signal acquisition was 30 min) (5). In normal individuals, no significant ^{18}F signal intensity difference was noted across gray matter regions compared pairwise across the cerebral midline, such as between right and left thalamus, or right and left striatum (comprising mostly part of putamen and body of the caudate nucleus), or across gray matter structures such as the cerebral cortex (sensorimotor area) compared with thalamus, or thalamus relative to striatum (left/right thalamus: 1.01 ± 0.03, range 0.95 to 1.04, $n = 6$, $P > 0.05$; left/right striatum: 0.99 ± 0.05, range 0.95 to 1.05, $n = 6$, $P > 0.05$; left cerebral cortex/ left thalamus: 1.04 ± 0.04, range 0.93 to 1.05, $n = 6$, $P > 0.05$; left thalamus/left striatum: 0.98 ± 0.04, range 0.96 to 1.02, $n = 6$, $P > 0.05$; example in Fig. 4, A and D). This was also the case for right to left differences in G1D (left/right striatum: 0.99 ± 0.03, range 0.94 to 1.04, $n = 6$, $P > 0.05$; left/right thalamus: 0.99 ± 0.03, range 0.94 to 1.03, $n = 6$, $P > 0.05$). In contrast, G1D individuals displayed a significant dissociation between striatal and thalamic signal (left thalamus/left striatum: 0.70 ± 0.09, range 0.57 to 0.83, $n = 6$, $P < 0.05$; example in Fig. 4, B and E) regardless of recent seizure occurrence. This suggested that the brain region distribution of the EEG source localization and BOLD-fMRI signal was associated with reduced glucose abundance at rest.

Mouse brain glucose and glycogen deficiency in G1D

With this information, we studied a stable antisense G1D mouse model that exhibits seizures, abnormal gait, and a clinically relevant (~50%) reduction in brain Glut1 transporter (17,18). Rather than relying on cerebrospinal fluid (CSF) glucose, which is substantially influenced by choroid plexus glucose filtration and therefore does not fully or solely reflect blood to brain transport nor the metabolic activity of neural cells (1, 19), we first performed ^{18}F-DG-PET under conditions of near metabolic steady state (20) to estimate the magnitude of brain glucose decrease for subsequent electrophysiological experiments. The amount of radiolabeled ^{18}F-DG intravenously administered was not significantly different between mouse groups (control, 43.5 ± 13.4 μCi, $n = 8$; G1D, 49.0 ± 11.8 μCi, $n = 8$, $P > 0.05$), as were pre- and post-PET blood glucose concentrations (initial control, 106 ± 35 mg/dl; initial G1D, 136 ± 79 mg/dl, $P > 0.05$; subsequent control, 196 ± 108 mg/dl; subsequent G1D, 211 ± 90 mg/dl; $n = 8$, $P > 0.05$). In contrast, the number of disintegrations per minute arising from brain relative to liver was different between groups (control, 79 ± 35; G1D: 49 ± 22 disintegrations per minute; $P = 0.04$; $n = 8$, $P < 0.05$; data file S2), yielding a G1D to control ^{18}F-DG signal ratio of about 62% (movie S4).

We complemented these results by performing ^{13}C mass spectrometry (MS) of the whole brain extracted again at near metabolic steady state after ^{13}C glucose intravenous infusion (20, 21). The percent molar enrichment for brain ^{13}C glucose was decreased in G1D (control, 0.56 ± 0.05, $n = 8$; G1D, 0.36 ± 0.03, $n = 7$; $P = 0.004$; data file S3), indicating that, in agreement with the fluorodeoxyglucose (FDG) results, at approximate metabolic equilibrium, the G1D brain contains about 63% of the blood-borne glucose that the control mouse harbors.

Decreased brain glucose can be expected to affect its storage as glycogen. To this end, fig. S6 illustrates the abundance of brain glycogen in the G1D brain in 14-week-old mice. Immunohistochemical staining with the anti-glycogen IV58B6 antibody and an amyloglucosidase based glycogen assay demonstrated reduced regional glycogen, as illustrated for the cerebral cortex, and significantly decreased total brain glycogen concentration (control, 1.44 ± 0.3 μmol glycogen/g tissue, $n = 4$; G1D, 0.65 ± 0.2 μmol glycogen/g tissue, $n = 4$; $P = 0.008$).

TCA neurotransmitter precursors in the G1D mouse brain

Among select TCA cycle intermediates and amino acids, only total acetyl coenzyme A concentration is slightly reduced in the G1D brain (18). Because this may affect neurotransmitter synthetic flux via reduced carbon availability, we measured the abundance of the main ^{13}C-glucose–derived coenzyme As in the brain as an indication of neurotransmitter precursor synthesis from blood-derived glucose (data file S3). Consistently with the previously noted magnitude of total acetyl coenzyme A decrease, there was only a modest reduction in the fraction of ^{13}C-glucose–derived acetyl coenzyme A in the G1D brain (control, 69.4 ± 21.9, $n = 8$; G1D, 52.3 ± 5.7, $n = 6$, $P < 0.05$; data file S3). These data indicate that despite reduced blood to brain glucose entry as illustrated by the ^{18}F-DG and ^{13}C glucose measurements above, the G1D brain is selectively carbon deficient from the point of view of acetyl coenzyme A concentration but retains at its disposal a normal

amount of other energy metabolism and neurotransmitter precursors. This result eliminated several possibilities as potential G1D epilepsy mechanisms such as overall brain energy failure. Thus, this led us to characterize, in a more focused manner, how neurons carry out neurotransmission as the most likely pathological process and to evaluate whether alternative sources of acetyl coenzyme A influenced it.

Excitation and inhibition in cortical pyramidal neurons

On the basis of the human G1D EEG source localization, BOLD-fMRI, and ^{18}F-DG-PET results above, we investigated the principal constituents of the thalamocortical circuit involved in absence seizures: somatosensory cortex, thalamic reticular nucleus (RT), and ventrobasal thalamus (VB). Whole-cell patch clamp recordings from layer V somatosensory cortical pyramidal neurons were used to evaluate synaptic inhibition and excitation in G1D mice. Glut1 expression increases during development, and in rodents, a switch in brain nutrient transporter expression from monocarboxylate to glucose transporters is complete by 27 postnatal (P) days (22). Therefore, we used neocortical slices from P35 to P45 animals. Under standard brain slice recording conditions, $GABA_A$ receptor (GABAR)–mediated, action potential–independent, miniature inhibitory postsynaptic currents (mIPSCs) recorded from G1D cortical neurons were similar to those from control in both frequency (3.33 ± 0.78 and 2.67 ± 0.57 Hz, respectively, $n = 9$ cells each, $P > 0.05$) and amplitude (20.28 ± 0.62 and 20.07 ± 0.80 pA, $n = 9$, $P > 0.05$) (Fig. 5A and data file S1). However, standard recordings are most often performed in high glucose [10 to 20 mM in artificial CSF (ACSF)] bath solution. However, CSF glucose concentration in G1D mice, with the caveat that this reflects brain tissue concentration only in part (1), is 1 to 1.5 mM (23), and elevated blood glucose ameliorates G1D seizures as shown above and in (11), and therefore, 10 to 20 mM glucose might suppress any synaptic deficits. A lower glucose concentration of 2.5 mM in ACSF results in a concentration of ~1.5 mM at 100 μm depth within the brain slice (24), which is the depth at which we recorded. Therefore, we studied mIPSCs after bath perfusion with 2.5 mM glucose containing ACSF. This revealed a reduction in mIPSC frequency in G1D cortical pyramidal neurons (G1D, 1.09 ± 0.27 Hz; $n = 12$; control, 2.67 ± 0.57 Hz; $n = 9$; $P = 0.013$, unpaired t test; Fig. 5B and data file S1). Average median synaptic event amplitudes were similar (G1D, 19.91 ± 0.51; control, 20.07 ± 0.80; $P > 0.05$; Fig. 5C and data file S1). This indicates that GABAR-mediated synaptic inhibition onto cortical neurons is diminished in G1D and that it is restored by elevated glucose. Thus, in all subsequent voltage-clamp experiments, unless stated otherwise, we compared electrophysiological properties of G1D neurons recorded in 2.5 mM bath glucose ACSF to those of control in 20 mM glucose.

To examine glutamatergic synaptic transmission, we assessed (a-amino-3-hydroxy-5-methyl-4-isoxazolepropionic acid AMPA) receptor (AMPAR)–mediated fast excitatory activity onto cortical neurons by recording miniature excitatory PSCs (mEPSCs) in the presence of the GABAR antagonist picrotoxin. This was similar between G1D and control (fig. S7A and data file S1). Mean mEPSC frequency of G1D cortical neurons was 1.30 ± 0.28 Hz ($n = 13$), similar to control neurons (1.96 ± 0.41 Hz, $n = 7$, $P > 0.05$; fig. S7B and data file S1). Similarly, the mean of median mEPSC amplitudes was comparable in G1D and control conditions (15.68 ± 0.39 and 16.57 ± 1.13 pA; $n = 13$ and 7, respectively; $P > 0.05$; fig. S7C and data file S1).

We then tested the metabolic dependence of mIPSC frequency. Ketogenic diets are used as therapy for G1D epilepsy (6). Their main ketone body by-products are β-hydroxybutyrate (BHB) and aceto-acetate. In ketone-consuming organs, BHB is converted to aceto-acetate, which in turn results in the formation of acetyl coenzyme A, which is diminished in the brain of G1D mice (18). We therefore replaced glucose (2.5 mM) with the fuel acetate (5 mM) and studied synaptic inhibition in thalamocortical (VB) neurons because, at this concentration, acetate and 2.5 mM glucose have similar acetyl coenzyme A carbon-donor capacity. After obtaining a baseline mIPSC recording, the perfusate was switched to acetate-containing ACSF. During the subsequent 10 min, mIPSC frequency increased in 66.7% of G1D neurons ($n = 4$) by 66.7% ($P < 0.05$, paired t test for neurons that exhibited a change) relative to no change in frequency in any control neurons ($n = 4$; $P > 0.05$, paired t test). The average mIPSC frequency in G1D neurons increased from 1.39 ± 0.25 to 2.13 ± 0.39 Hz ($P = 0.048$, paired t test; Fig. 5C and data file S1), indicating restoration when compared with control under 2.5 mM glucose.

Diminished inhibitory action in the context of unaltered excitatory conductance in G1D cortical neurons likely reflects excitation/inhibition balance. We tested this possible imbalance by determining the input/output relationship of evoked (e) IPSCs and EPSCs obtained from the same neuron. eIPSCs and eEPSCs were obtained under increasing stimulation intensities to construct input/output curves as shown in fig. S7D and data file S1. With increasing stimulus strength, G1D excitatory currents increased sharply relative to inhibitory currents. In contrast, excitatory currents increased gradually and by smaller magnitude in control neurons compared to G1D before reaching a maximum, revealing a more robust inhibitory counteraction of excitation (fig. S7E and data file S1). Rapid increase of mIPSCs with high glucose or fuel substitution is compatible with defective presynaptic function. To investigate this, we assessed electrically evoked GABAR synaptic transmission onto G1D cortical neurons by stimulating layers II and III of the cortex. A pair of electrical stimuli separated by 25 ms resulted in increased amplitude of the second response in G1D cortical neurons but not in control ($n = 5$; fig. S7, F and G, and data file S1). This facilitation likely indicated reduced presynaptic GABA release probability in G1D. Overall, these findings indicate that G1D layer V somatosensory cortical neurons experience fuel-dependent reduction in inhibition, likely rendering them susceptible to generate or propagate seizures.

Phasic and tonic inhibition of thalamic relay neurons

In other absence seizure models, enhanced excitatory input from corticothalamic (CT) terminals can recruit oscillatory thalamocortical relay (VB) neuron activity. This may occur either via direct activation of the cortico-RT pathway or by activation of the cortico-TC (thalamocortical)-RT pathway, facilitating RT-mediated feed-forward inhibition–induced T-type Ca^{2+} channel–dependent burst firing (25). Enhanced tonic inhibition via activation of extrasynaptic GABARs is considered a common mechanism in such absence seizures (26). TC relay neurons in the ventrobasal nucleus exhibit robust tonic chloride conductance mediated by extrasynaptic α4β2δ subunit–containing GABARs (27). Elevated extracellular GABA (26) due to thalamic GABA transporter type 1 (GAT1) dysfunction probably underlies such enhanced tonic inhibition in animal models of absence seizures

(28). There is astrocytosis in G1D (18), which could be associated with diminished GAT function. We therefore examined tonic GABAR current amplitude from TC relay neurons in thalamic slices from G1D and control animals by determining the shift in baseline holding current after application of the GABAR antagonist bicuculline (100 μM) in the presence of glutamatergic antagonists and without GABA uptake blockers. Reflecting the presence of the tonic current, application of bicuculline to brain slices caused an inward shift in baseline holding current in both G1D (46.34 ± 9.01; $n = 6$ cells; four mice) and control TC neurons (47.64 ± 7.87 pA; $n = 9$ cells; six mice; $P > 0.05$, unpaired t test; Fig. 6, A and B, and data file S1) without appreciable change when G1D slices were perfused with 20 mM glucose [39.74 ± 7.31 pA; $n = 13$ cells; five mice; $P > 0.05$, one-way analysis of variance (ANOVA)], indicating that tonic inhibition in G1D TC neurons is unaltered by glucose. Normalized to cell capacitance, the magnitude of tonic current in G1D neurons (3.46 ± 0.70 pA/pF) was similar to control (4.48 ± 0.70 pA/pF; $P > 0.05$, unpaired t test; Fig. 6C and data file S1), suggesting that, unlike other absence seizure models, baseline tonic inhibition is unaltered in G1D relative to control and independent of the glucose concentrations tested.

To investigate whether IPSCs were diminished in the VB thalamus, we compared GABAR-mediated spontaneous inhibitory postsynaptic currents (sIPSC) in G1D TC neurons with control (Fig. 6, A and D, and data file S1). sIPSC frequency was reduced by 64% in G1D TC neurons (1.63 ± 0.80 and 4.50 ± 0.83 Hz, respectively; $n = 6$; $P < 0.05$, unpaired t test; Fig. 6, D, E, and I, and data file S1), with similar event amplitude (56.28 ± 12.8 and 57.86 ± 11.35 pA, respectively; $n = 6$; $P > 0.05$, unpaired t test; Fig. 6J and data file S1). In both G1D and control VB neurons, individual synaptic events were randomly interspersed with bursts of sIPSCs, suggestive of high-frequency discharges of the RT releasing GABA onto VB synapses (Fig. 6A and data file S1) (29). To quantify differences in IPSC bursts between G1D and control neurons, we defined bursts as a series of four consecutive IPSCs detected within 30 ms of each other in low-pass-filtered (100 Hz) recordings (30). In recordings summarized in table S1, G1D and control VB neurons exhibited similar numbers of IPSC bursts per minute, IPSCs per burst, burst durations, and interburst intervals ($P > 0.05$, t test with Welch correction for all four G1D to control comparisons). These findings demonstrate that, despite a general reduction in phasic inhibitory input to VB neurons, RT burst discharge–mediated GABA release onto VB relay neurons is preserved in G1D.

To evaluate the effect of glucose on synaptic inhibition onto control TC neurons, after recording for 10 min in 20 mM glucose ACSF, we switched perfusion to 2.5 mM glucose ACSF and recorded for a further 40 min. Cells were discarded if access resistance increased by more than 20% during the final 40 min of recording. This reduction in glucose resulted in a significant decrease in sIPSC frequency to 28.2% of the frequency in 20 mM glucose ($n = 5$ cells; $P < 0.05$, one-sample t test), with no effect on sIPSC amplitude ($P > 0.05$, one-sample t test; table S2). These findings indicate that, whereas diminished glucose impairs inhibitory transmission onto TC relay neurons in both control and G1D, the magnitude of reduction of inhibitory transmission is greater in G1D.

Glucose and ketone body effects on thalamic phasic synaptic inhibition

We next tested whether perfusion with 20 mM glucose ACSF also modulated phasic GABAR-mediated synaptic inhibition onto G1D TC relay neurons. Mean sIPSC frequency was 4.20 ± 0.65 Hz (n = 24), similar to control (4.31 ± 0.84 Hz; n = 18; P > 0.05, unpaired t test; Fig. 6, D to F, and data file S1), confirming that elevated glucose normalizes synaptic inhibition onto G1D TC neurons. We also tested whether BHB addition to 2.5 mM glucose containing ACSF modulated synaptic inhibition onto G1D TC neurons. We used this supplementation because replacement of glucose with hydroxybutyrate can decrease neuronal activity (31). After obtaining baseline sIPSCs in 20 mM glucose ACSF for 10 min, slices were perfused with 2.5 mM glucose ACSF supplemented with 2.5 mM BHB, and sIPSCs were monitored for a further 40 min (Fig. 6, F to H and L, and data file S1). G1D and control TC neurons exhibited different responses to BHB. In G1D TC neurons (n = 7), 20 min after perfusion with BHB, sIPSC increased by 16% (Fig. 6L, time point 30 min; P < 0.05, two-way ANOVA; data file S1). By 40 min after the perfusion change, event frequency became twofold greater than at baseline (P < 0.05, two-way ANOVA). In contrast, and similar to other studies (32), BHB perfusion did not prevent glucose deprivation–induced sIPSC run-down on control TC neurons (n = 7) where, compared to baseline, event frequency was 54% reduced (Fig. 6L, time point 50 min; P < 0.05, two-way ANOVA; data file S1). Thus, either raised glucose or ketone body supplementation reversed the inhibition deficit in G1D.

Glutamatergic synaptic transmission onto thalamic relay neurons

Spontaneous EPSCs (sEPSCs) were recorded by voltage clamping neurons to −65 mV in the presence of 5 mM extracellular Mg^{2+}, thus ensuring that the recorded EPSCs were predominantly mediated by AMPAR activation. As shown in fig. S8A and data file S1, comparison of sEPSCs obtained from control and G1D revealed essentially unchanged excitatory input onto G1D TC neurons (n = 6). Specifically, there was no difference in sEPSC frequency in G1D TC neurons relative to control (2.8 ± 0.42 and 1.76 ± 0.23 Hz, respectively; n = 6 for both control and G1D; P = 0.061, t test; fig. S8, B to D, and data file S1). sEPSC amplitude (14.2 ± 1.6 and 15.9 ± 0.96 pA) and decay (3.50 ± 0.31 and 3.16 ± 0.16 ms) were also similar for the two groups. Perfusing G1D brain slices with 20 mM glucose did not alter sEPSC frequency in VB neurons compared to control (1.83 ± 0.37 and 1.76 ± 0.23 Hz, respectively; n = 6 for both; P > 0.05, t test). Likewise, exposing control TC neurons to 2.5 mM glucose did not affect sEPSC frequency (1.76 ± 0.23 and 1.71 ± 0.5 Hz, respectively; n = 6 for both, P > 0.05) or amplitude (15.89 ± 0.96 and 16.87 ± 1.49 pA; P > 0.05) but prolonged current decay (3.16 ± 0.16 and 4.28 ± 0.41 ms; P = 0.013, t test).

Low threshold spiking and tonic firing of thalamic relay neurons

Low-voltage activated, transient (T-type) thalamic Ca^{2+} channels mediate characteristic bursts of low-threshold spikes (LTSs) and participate in vigilance and seizures (33). Most LTS during spike-wave discharges are associated with a change in firing patterns from tonic firing to burst firing. Therefore, we tested LTS in G1D by quantifying burst firing response to hyperpolarizing or depolarizing current steps. Prolonged hyperpolarizing negative currents (1.5 s), which maximize T-type Ca^{2}+ channel de-inactivation, evoked a

post-inhibitory rebound (PIR) in control VB neurons that appeared in G1D VB neurons (2.5 mM glucose) as shown in fig. S9A and data file S1. Two of eight (25%) G1D VB neurons exhibited PIR with a mean current injection necessary to evoke PIR of −190 ± 10 pA. This current hyperpolarized the membrane potential to −78.2 ± 1.4 mV, after which the rebound occurred with a latency of 84.73 ± 4.17 ms (4 ± 2 action potentials per burst). In contrast, control VB relay neurons ($n = 9$) displayed PIR with a lower threshold current of 105.6 ± 13.2 pA that hyperpolarized the neurons to −78.48 ± 3.5 mV. Cessation of hyperpolarization led to PIR (5.63 ± 1.05 action potentials per burst) after 150.1 ± 22.5 ms. PIR absence or higher PIR threshold in G1D VB neurons was associated with a more hyperpolarized resting membrane potential in G1D neurons (−73.7 ± 2.58 versus −65.88 ± 0.94 mV, respectively; $P = 0.01$, unpaired t test) and unaltered input resistance (G1D versus control: 113.4 ± 22.9 and 90.7 ± 17.8 megohms, respectively; $P > 0.05$). Hyperpolarizing control or G1D VB neurons to membrane potentials greater than −70 mV (in 20 mM glucose) also suppressed PIR, suggesting that the apparent suppression of PIR in G1D neurons was likely due to inactivation of T-type Ca^{2+} channels. We therefore studied changes in LTS in response to depolarizing current injection (fig. S9, A and B, and data file S1). LTS evoked in eight G1D (2.5 mM glucose) and nine control VB neurons exhibited similar characteristics, including threshold current (196.7 ± 36.3 versus 141.3 ± 36.4 pA; fig. S9B and data file S1), onset latency (56.45 ± 13.61 versus 88.89 ± 14.91 ms; fig. S9C and data file S1), number of action potentials per burst (3.167 ± 0.54 versus 4 ± 0.68 mV) (fig. S9D and data file S1), and frequency (91.52 ± 17.04 versus 130.9 ± 8.11 Hz; fig. S9E and data file S1).

We next tested whether tonic firing was altered in G1D VB neurons by injecting long depolarizing currents of increasing magnitude (fig. S9, F to I, and data file S1). Tonic firing was similar in eight G1D VB neurons perfused with 2.5 or 20 mM glucose, and similar to nine control neurons. The threshold current required to evoke tonic firing was similar in G1D VB neurons perfused with 2.5 mM (205 ± 50.6 pA) or 20 mM (134.3 ± 40.5 pA) glucose, whereas in control it was 221.4 ± 38.39 pA ($P > 0.05$, one-way ANOVA; fig. S9F and data file S1). At threshold, the average number and frequency of action potentials were similar between G1D and control VB neurons (fig. S9G and data file S1). Figure S9H and data file S1 illustrate that the firing frequency with increasing step currents was similar across the three groups (control slope, −1.12 ± 1.03; G1D in 2.5 mM glucose slope, 1.47 ± 0.69; G1D in 20 mM glucose slope, 2.75 ± 0.35; $P > 0.05$, one-way ANOVA). Similarly, the instantaneous frequency of action potentials at threshold in G1D (2.5 and 20 mM glucose) and control VB neurons was unchanged (10.65 ± 4.65, 13.78 ± 1.96, and 11.75 ± 3.68 Hz; $P > 0.05$, one-way ANOVA; fig. S9I and data file S1). Compared to control VB neurons, spike frequency adaptation under increasing magnitudes of current injection, evidenced by increasing variance in firing frequency during repetitive spiking, was less pronounced in G1D VB neurons regardless of ACSF glucose concentration. However, average firing frequency for the overall population was similar between G1D and control VB neurons, suggesting unaltered LTS and tonic firing properties in G1D VB neurons. Figure S9J and data file S1 illustrate differences among the three groups in resting membrane potential (control, −66.12 ± 0.98 mV, $n = 12$; G1D 2.5 mM glucose, −63.82 ± 3.01 mV, $n = 14$; G1D 20 mM glucose, −70.67 ± 1.21 mV, $n = 14$; $P > 0.05$, t test; fig. S9J and data file S1) and input resistance (control, 91.69 ± 11.02 megohms, $n = 10$; G1D 2.5 mM glucose,

78.58 ± 10.18 megohms, $n = 8$; G1D 20 mM glucose, 105.40 ± 22.25 megohms, $n = 8$; $P > 0.05$, *t* test; fig. S9K and data file S1). Figure S9L and data file S1 show that the excitatory postsynaptic potential (EPSP) frequency onto G1D VB neurons is increased when slice is perfused with 2.5 mM [control, 7.88 ± 0.55 Hz, $n = 7$; G1D 2.5 mM glucose, 12.99 ± 1.84 Hz, $n = 11$; G1D 20 mM glucose, 9.88 ± 0.86 Hz, $n = 11$; $P < 0.05$ compared to wild type (WT), *t* test]. Figure S9M and data file S1 show paired plots obtained from fig. S9L and data file S1 before and after perfusion of 2.5 mM glucose, indicating that when extracellular glucose availability is reduced, VB relay neurons experience increased frequency of EPSPs (control, 7.87 ± 0.55 Hz, $n = 7$; G1D 2.5 mM glucose, 12.99 ± 1.84 Hz, $n = 8$; G1D 20 mM glucose, 9.88 ± 0.86 Hz, $n = 8$; $P < 0.05$ compared to G1D 20 mM glucose, unpaired *t* test).

Firing of thalamic reticular neurons

Diminished synaptic inhibitory neurotransmission suggested excitation/inhibition imbalance on VB neurons arising from loss of feed-forward inhibition mediated by RT neurons. Therefore, the impact of Glut1 insufficiency on RT neuronal excitability was determined in current clamp recordings (Fig. 7 and data file S1). Figure 7A illustrates recordings for RT neurons of control, G1D in 2.5 mM glucose and G1D in 20 mM glucose, in response to depolarizing current steps. The recordings were first obtained in 20 mM glucose followed by perfusate containing 2.5 mM glucose. Control RT relay neurons did not tolerate decreased glucose in current clamp mode. In contrast to G1D neurons, transitioning from 20 to 2.5 mM glucose irreversibly depolarized all the control RT neurons ($n = 8$ neurons, from −65.69 ± 0.98 mV to complete depolarization with loss of membrane resistance for these conditions). Reverting to 20 mM glucose ACSF did not counteract depolarization. Hence, studies in control neurons were conducted in 20 mM glucose.

We evaluated LTS generated by RT neurons (Fig. 7, B to E), which were exhibited by both G1D (5 of 8 cells) and control (8 of 10 cells). Among the neurons that displayed LTS, G1D cells were slightly more hyperpolarized than control (−75.46 ± 1.42 versus −70.02 ± 1.45 mV; $P = 0.02$, unpaired *t* test). The patterns of burst firing were more variable in control RT neurons than in G1D. The LTS latency to onset (95.51 ± 19.75 versus 103.7 ± 25.97 ms; $P > 0.05$, unpaired *t* test; Fig. 7C), the number of action potentials per burst (4.2 ± 0.58 versus 16.14 ± 5.65, respectively; $P > 0.05$, unpaired *t* test; Fig. 7D), and LTS frequency (80.91 ± 5.05 versus 128.50 ± 24.60 Hz; $P > 0.05$, unpaired *t* test; Fig. 7E) were similar between G1D and control RT neurons. Although the threshold current needed to elicit tonic firing was also similar between the two groups (90.00 ± 22.80 versus 74.29 ± 15.71 pA; $n = 5$ and 7, respectively; $P > 0.05$, unpaired *t* test; Fig. 7F), tonic firing of G1D RT neurons was reduced relative to control. Average firing tonic firing frequency at threshold in G1D RT neurons was 23.74 ± 16.58 Hz ($n = 5$), whereas in control it was 89.43 ± 21.3 Hz ($n = 7$; $P = 0.047$, unpaired *t* test; Fig. 7G). Perfusion of G1D brain slices with 20 mM glucose modified tonic firing frequency of G1D RT neurons toward control values (45.52 ± 17.60 versus 89.43 ± 21.30 Hz; $n = 13$ and 7, respectively; $P = 0.04$, unpaired *t* test; Fig. 7G). Figure 7H illustrates that the firing frequency with increasing step currents was similar across the three groups (control slope, −0.97 ± 0.48; G1D in 2.5 mM glucose slope, −0.18 ± 0.34; G1D in 20 mM glucose slope, 0.33 ± 0.29; $P > 0.05$, one-way ANOVA). Diminished tonic firing in these G1D RT neurons was not due to a difference in instantaneous firing

frequency in G1D RT neurons (26.77 ± 16.58 versus 110.9 ± 32.41 Hz; $P = 0.06$, unpaired t test; Fig. 7I), and perfusion of G1D RT neurons with 20 mM glucose did not affect the results (59.27 ± 21.3; $P = 0.18$, compared to control, unpaired t test; Fig. 7I). These results suggest that tonic firing of RT neurons in response to depolarizing input is diminished in G1D. RT neurons displayed similar resting membrane potential (G1D, −66.50 ± 2.65 mV; $n = 10$ versus control, −65.69 ± 0.98 mV; $n = 11$; $P > 0.05$, unpaired t test; Fig. 7J) and input resistance (G1D, 78.58 ± 10.18 megohms; $n = 8$ versus control, 91.69 ± 11.02 megohms; $n = 10$; Fig. 7K). However, similar to VB neurons (fig. S9L), G1D RT neurons received more spontaneous EPSPs (13.28 ± 1.90 versus 8.20 ± 0.61 Hz; $P = 0.037$, unpaired t test; Fig. 7, L and M).

Ketone body prevention of G1D mouse seizures

In addition to absence, G1D includes both generalized tonic clonic or convulsive seizures (GTCSs) (6), which can be the first disease manifestation (34) and convulsive status epilepticus (SE) (9). None of these seizure types were spontaneously apparent in this mouse model. We therefore determined the susceptibility of G1D mice to GTCS induced by the muscarinic agonist pilocarpine (35) by determining the dose-response relationship for GTCS [Racine scale (36)] in G1D and control mice within 100 min of an intraperitoneal pilocarpine injection. At all doses tested, GTCS occurred earlier and in a greater proportion in G1D mice (Fig. 8A). The data were fit with a sigmoidal function that revealed a shift to lower doses for induction of GTCS in G1D. The dose needed to induce GTCS in 50% of animals (ED_{50}) was 182.2 mg/kg for control, in contrast with 141.5 mg/kg for G1D ($P < 0.05$). At ED_{100} dose (270 mg/kg), GTCS rapidly progressed into convulsive SE in both G1D and control animals with lethality for all mice within 3 hours of seizure onset (Fig. 8A).

Because the results above suggest that ketone bodies can restore GABAergic synaptic currents, we tested the hypothesis that ketone bodies increase the threshold to pilocarpine-induced GTCS. We pretreated G1D animals with β-ketopentanoate (BKP; 200 mg/kg, intraperitoneally), a ketone derived from the metabolism of heptanoic acid or triheptanoin (37), before pilocarpine administration. None of the G1D animals ($n = 12$) pretreated with BKP experienced pilocarpine-induced GTCS. In contrast, pilocarpine-induced GTCS occurred in 66.7% (8 of 12) of untreated mice (Fig. 8B), suggesting that ketone bodies raise seizure threshold in G1D.

Pharmacological GABA and AMPAR modulation effects on G1D seizures

Several antiseizure drugs used for treatment of childhood seizures and SE including GABAergic agents (phenobarbital and diazepam) and valproate are weak in vitro inhibitors of Glut1 (38-40) and are thus not recommended for individuals with G1D (41). However, these data derive from studies that use elevated drug concentrations applied to isolated cells. Thus, we determined the efficacy of various drugs including the diazepam to terminate GTCS in the G1D mouse.

We first tested diazepam administered at an early time t1 (within 5 min of seizure onset) or at an established phase, t2 (30 min after seizure onset). Seizure termination was defined

as the cessation of observable convulsions, myoclonus or postural immobility, and staring activity over 3 hours. Increasing doses of diazepam were administered intraperitoneally either within 1 min of seizure onset (t1) or 30 min later (t2). Prolonged pilocarpine-induced SE results in diazepam refractoriness (42). Dose-response analysis in control animals at t1 and t2 confirmed that, with increasing SE duration, the ED_{50} value for diazepam to terminate seizures increased from 0.90 mg/kg when administered within 1 min (t1) to 24.8 mg/g when administered at 30 min of seizures (t2) (Fig. 8C). We then studied the efficacy of diazepam to terminate early SE. Treatment of G1D mice with diazepam (1 mg/kg) terminated SE in only 2 of 10 mice (20%). Higher dose (3 mg/kg) did not alter outcome, as SE was terminated in only 2 of 11 animals (18.2%). In control mice, diazepam exhibited dose-dependent efficacy in terminating SE (1 mg/kg; 75% efficacy; $n = 8$ and 3 mg/kg; 100%; $n = 8$) (Fig. 8D). Diazepam at either 30 mg/kg ($n = 4$) or 50 mg/kg ($n = 5$) failed to abort established SE in G1D mice. In contrast, diazepam terminated established SE in 50% (30 mg/kg; $n = 6$) or 71.4% (50 mg/kg; $n = 7$; Fig. 8E) of control mice.

Because the anticonvulsant activity of diazepam is influenced by the clinical and electrographic stage of seizures (42) and because electrographic seizures can occur in the absence of visible manifestations, we further tested the effect of early diazepam treatment on electrographic seizures. After obtaining a 20-min baseline EEG from implanted hippocampal electrodes, G1D ($n = 5$) and control ($n = 6$) mice, we treated them with diazepam (3 mg/kg, intraperitoneally) within 30 s of the onset of electrographic seizures. EEG was continuously recorded for 24 hours. Sample EEG traces are displayed in Fig. 8F. In all G1D mice, EEG seizures were observed for several hours after transient seizure suppression as evidenced by high-frequency continuous spiking lasting more than 1 hour (Fig. 8F). By 20 hours after onset (Fig. 8F, bottom), seizures evolved into periodic epileptiform discharges in all the mice, suggesting that neuronal damage had occurred. SE was terminated within 5 min after diazepam treatment in all control mice, and recurrence was not observed over 24 hours. In contrast, diazepam did not prevent the progression of SE in G1D mice, indicating that diazepam is ineffective against GTCS and SE in G1D mice.

We next studied the efficacy of phenobarbital on GTCS in G1D mice. Dose-response studies performed in control mice revealed that ED_{50} values for phenobarbital to terminate seizures increased from 71.1 mg/kg when administered within 1 min of GTCS (t1) to 90.9 mg/kg when administered during established SE (Fig. 8G). Use of phenobarbital above 50 mg/kg induced respiratory depression in G1D mice. Therefore, we used a single dose (50 mg/kg). The sensitivity to early treatment of GTCS with phenobarbital was similar in G1D (71.4%; $n = 7$) and control (66.7%; $n = 6$) mice (Fig. 8H). In contrast, phenobarbital aborted established SE in only 16.7% of G1D mice ($n = 6$) and 44.4% of control mice ($n = 9$). This suggests that phenobarbital can effectively treat GTCS only when administered early and with the associated risk of respiratory depression and is ineffective in treating established SE in G1D.

Given the failure of GABAergic drugs to counteract GTCS in G1D mice, which is also observed in individuals with G1D (41), we next sought to reduce excitation. The AMPAR-kainate receptor antagonist GYKI-52466 can terminate diazepam refractory GTCS (43). We therefore tested the efficacy of a standard dose of GYKI-52466 (50 mg/kg, intraperitoneally)

(43) on GTCS in G1D mice (Fig. 8I). GYKI-52466 terminated both early (six of seven mice) GTCS and established SE (six of seven) in G1D mice. This effect was not associated with substantial respiratory depression, thus suggesting that AMPAR block is a potential therapeutic target for the treatment of GTCS in G1D.

DISCUSSION

Despite the paradoxical relationship between reduced metabolism and hyperexcitability characteristic of numerous neurometabolic diseases, the evidence previously available for G1D has not allowed for mechanistic neurophysiological inferences: Human G1D seizures are generally refractory to antiseizure drugs (44) perhaps, at least in part, because some are in vitro inhibitors of Glut1 (38-40), obscuring attribution to specific molecular mediators. In this context, a survey of the salient human brain regions most relevant for G1D seizures by nonlinear EEG signal source analysis and by simultaneous EEG-fMRI revealed seizure onset and robust ictal BOLD activation in sensorimotor cortex and thalamus among other structures less often implicated in epilepsy. This was correlated with ^{18}F-DG-PET, which demonstrated reduced tracer accumulation in the thalamus relative to the striatum together with decreased cortical and cerebellar signal.

Using a G1D mouse model (18, 37), we noted decreased brain ^{18}F-DG accumulation and glycogen content but normal glucose-derived TCA cycle coenzyme A intermediates other than acetyl coenzyme A. In contrast with our original model (23), this model is more faithful to the human syndrome because it displays a reduction in cerebral Glut1 comparable to the effect of some heterologously expressed human mutations and to human G1D red blood cells (17), with frequent electrical oscillations in thalamocortical brain slices under reduced glucose, electrographic seizures, and profound ataxia (18, 37). The barrel somatosensory cortex and the thalamus provided a test bed to elucidate the synaptic activity basis of hyperexcitability and its metabolic dependence and antiseizure drug response. These regions have received attention in epileptology because they constitute a hypersynchronized circuit during absence-like seizures of other causes (29, 45, 46). In contrast with those epilepsies, which are characterized by loss of tonic inhibition (26), in G1D phasic or neural activity–dependent synaptic GABAergic inhibition was diminished in both cortical and thalamic regions, with glutamatergic synaptic excitation remaining either unaltered or modestly enhanced in the cortex and the thalamus, respectively.

The results indicate that hyperexcitability in G1D is consequent to neural cell dysfunction rather than simply reduced blood-brain barrier glucose influx, and dependent on or rate-limited by glucose, suggesting loss of the normal adaptive mechanism to fluctuations in blood glucose that, we postulate, stems from depletion of brain glycogen, perhaps via a decreased capacity to sustain neural activity from glycogen conversion to glucose (47). Furthermore, G1D seizures are associated not with downstream energy precursor deficiency or failure but with a defect in the GABA released during phasic neurotransmission onto CT and thalamocortical relay neurons. Notably, the abnormal synaptic activity and seizure susceptibility are reversible with metabolic fuels such as glucose, acetate, or ketone bodies, indicating that hyperexcitability in G1D is a functional reversible state.

As a first approximation, the selective inhibitory neurotransmission deficit characteristic of G1D may have been consequent to diminished GABA synthesis or decreased GABA release at the synapse. De novo synthesis of glutamate and derived GABA relies on the TCA cycle, which supplies both carbon and energy. A modest reduction of acetyl coenzyme A in G1D accompanies otherwise preserved TCA intermediates and glutamate and GABA brain content (18) such that overall GABA synthetic failure is unlikely but synaptic vesicular release defective. In this context, the blood glucose concentration dependence of seizures in G1D individuals suggests that this process has become dependent on mass action from blood to brain. This stands in contrast with normal individuals, in which there is no such dependence unless exposed to extremely low blood glucose concentration. Both hypoglycemia and hyperglycemia may be unnoticed (48). We postulate that this heightened dependence on blood glucose is due to depletion of glycogen, which serves as a source of glucose under conditions of elevated neural activity (47). The additional finding of decreased (about 62% of normal) brain glucose content in G1D supports this notion, because comparable decreases in glycolytic flux are disease causing via excitable dysfunction (49). In this contention, decreased brain glucose entry and reduced glycogen content could prove intermittently insufficient to maintain balanced excitability or fail to counteract, via glycolysis, episodic seizure generation due to other unknown factors, resulting in an oscillatory electrical discharge.

The occurrence of spike-wave seizures with rapid electrographic generalization in G1D individuals had precluded attribution to a discrete cerebral source or focus. Our source localization estimation coupled with fMRI and PET results indicates that ictal events occur in a regionally abnormal brain both ictally and interictally primarily involving the thalamocortical circuit. However, a substantial fraction of seizures does not alter consciousness, including attention-demanding activities such as reciting a number sequence. Some theories of consciousness are incompatible with our observations. In them, the performance of a task requires the “binding” of dissociated information received through the senses by the integrative action of thalamocortical circuits (50). This derives from the notion that, because specific neurons respond to sensory and other aspects such as form and movement, objects or other aspects of experience or volition must be codified and separated by the brain into constituents (51), which need assembling for unified perception or conception. This is apparently supported by the finding of excess synchronization of the EEG despite preservation of sensory nerve response under increasing anesthesia (52) and by the excessive synchronization typical of seizures with loss of consciousness (53). However, the cited theories cannot be reconciled with our results. This is not simply a case of experimental discrepancy because the term binding as used in these theories incurs into the mereological fallacy, which consists in ascribing to the brain attributes or actions that refer only to the human being as a whole (54, 55).

Our results in brain slices, which are exposed to varying glucose concentration in independence of the blood-brain barrier, indicate that neural cells constitute an important disease locus. Disease remediation approaches based on gene or Glut1 protein augmentation therefore need to account for this phenomenon. In contrast with neurons, glial cells and also red blood and endothelial cells are rich in Glut1. Further work will be necessary to discern the quantitative contribution of these cellular compartments to the process of

brain glucose entry, as these considerations become particularly relevant for augmentation treatments because the opposite phenomenon, namely, increased Glut1 expression, is associated with signaling dysregulation leading to nephropathy (56), retinopathy (57), and advanced-glycation end-product–mediated neural toxicity (57).

Thalamocortical oscillations are a characteristic cerebral rhythm identified in several normal and disease states (25). Despite reductionist assumptions that intrinsic neuronal neurophysiological properties may be used to predict oscillation properties (58), thalamic circuit activity is influenced by events as diverse as behavioral vigilance or sleep (59), and the consequences of specific synaptic dysfunction are not always predictable a priori. Furthermore, inhibitory neuron proportion differences exist between higher and lower mammals (60). Nevertheless, slow frequency oscillations in thalamic neurons are at least in part responsive to cortical generation (61). Abnormal cerebral cortical activity is important for the genesis of absence seizures in general, as increased EEG spectral power precedes spike-wave discharges in the S1 region of the rodent somatosensory cortex (62). Layer V pyramidal neurons project to layer VI (CT) neurons, which in turn project to the thalamus (63). Thus, changes in the properties of the local cortical microcircuit can render CT neurons susceptible to triggering or maintaining pathological spike wave discharges (64). Layer V parvalbumin–positive interneurons, which constitute the major perisomatic inhibitory input to layer V pyramidal cells and critically modulate their firing output (65), exhibit elevated energy consumption (66) and increased susceptibility to energetic deficit (67). We therefore propose that impaired interneuron function in G1D leads to diminished inhibitory output, altering excitation/inhibition balance in cortical neurons and favoring spike-wave initiation and propagation to the thalamus.

The reversal of reduced sIPSC frequency after perfusion with ACSF containing high glucose or BHB in G1D is consistent with augmentation of synaptic GABA release due to increased fuel availability. However, despite the overall reduction in sIPSC frequency, the occurrence of IPSC bursts on VB neurons indicates preservation of burst firing output of RT, which can generate pathologic thalamocortical rhythms. This is substantiated by the ability of G1D RT neurons to generate robust LTS. G1D thalamocortical slices, unlike those prepared from other absence epilepsy models, exhibit ~3-Hz thalamocortical oscillations (18). The RT is essential to the generation of 7- to 11-Hz thalamocortical oscillations (62). Lesions of the RT that preserve the VB thalamus in WAG/Rij rats result in frequent de novo slower paroxysmal oscillations at 3 to 5 Hz, a rhythm that is closer to the intrinsic rhythmic bursts from VB relay cells at 2 to 4 Hz (68). These findings indicate that, as in the RT lesioned WAG/Rij animals, spike-wave discharges in G1D may be driven by excitatory currents arising from cortical pyramidal neurons to the VB relay neurons rather than by inhibitory input from the RT.

In this context, given our finding of diminished GABA release, it is expected that tonic inhibition is unaltered in G1D. Vesicular GABA release can influence the magnitude of tonic inhibition on TC relay neurons (69). The preservation of tonic inhibition on G1D VB neurons despite reduced phasic inhibition onto them suggests that either GABA release from RT neurons is sufficient to maintain the concentration of ambient or extracellular GABA necessary to activate the high-affinity slowly desensitizing extrasynaptic GABARs (70) , or

that extrasynaptic GABARs are up-regulated. The latter is unlikely given that normalization of phasic inhibition with 20 mM glucose does not alter the magnitude of tonic inhibition. This suggests that, in contrast with most absence epilepsies, but analogously to the tottering (26) or the heterozygous GABAR α1 subunit knockout (71) models, G1D is not associated with an increase in basal GABAR-mediated tonic inhibition. Nevertheless, during tonic firing of RT neurons, baseline holding current mediated by extrasynaptic GABARs on VB neurons is enhanced (72). Our observation in G1D of preserved putative burst-induced GABA release at RT-VB synapses and intact intrinsic firing properties of RT neurons suggests that tonic inhibition onto VB neurons may constitute a potential anti-seizure target in G1D.

The differences between G1D and other absence epilepsy mechanisms also extend to clinical observations. Whereas pharmacological amelioration of EEG seizures in absence epilepsy of other causes is not necessarily associated with cognitive benefit (73), this is not the case for G1D, where dietary therapy can affect both electrographic and cognitive aspects (8).

We propose that the ^{18}F-DG-PET thalamus-striatum signal ratio is endowed with diagnostic value. This ratio is ~0.7 in G1D, whereas in the normal brain the ratio is ~1. It has been known for over 20 years that ^{18}F-DG-PET is characteristically informative in G1D, and this constituted the first evidence that brain glucose content was decreased in the disorder across a broad age range (5). This characteristic PET pattern becomes more relevant for a fraction of individuals with robust clinical and analytical features of G1D who harbor nondiagnostic or misinterpreted variants in the *slc2a1* gene (6, 74). However, further work will be necessary to elucidate the specificity of this finding, particularly if milder disease phenotypes emerge or if a second causal gene was found.

Ketogenic diets are used to treat G1D and other epilepsies (41), however incompletely (9). This treatment modality probably stimulates or represses an array of mechanisms, some of which may occur at the appropriate time frame and magnitude to benefit G1D individuals (75). These diets, however, are poor in anaplerotic potential (which is the capacity for TCA cycle precursor or net carbon replenishment), but this can be circumvented by the use of specific dietary metabolic substrate (8, 37). The seizure amelioration observed with these diets in G1D can be explained because extra glucose or ketone bodies augment brain acetyl coenzyme A production (37), normalizing neurotransmitter release. This contention can also explain why seizures in G1D predominate in childhood, when brain glucose utilization is greatest, and usually resolve after adolescence, when glucose utilization decreases (9). Further investigation of this approach is supported by our results, specifically whether our findings of diminished GABA release in G1D and subsequent normalization by enhancing glycolysis (using glucose containing ACSF) or fueling the TCA cycle (using acetoacetate or BHB) are an indication that impairment of synaptic activity–dependent adenosine triphosphate (ATP) synthesis through glycolysis and oxidative phosphorylation may constrain vesicular cycling (76), thus depressing synaptic inhibitory neurotransmission. In the setting of GABAR modulation failure, inhibition of AMPAR [for example, using perampanel (77)] emerges as a potential treatment for G1D given its ability to terminate severe early and established seizures.

Numerous epilepsies are associated with increased excitation due to enhanced glutamatergic activity (37). In contrast, disinhibition characterizes G1D. In the related epileptic glucose metabolic disorder pyruvate dehydrogenase deficiency, reduced glutamate also coexists with neuronal inhibitory failure, which permits excessive excitatory neuron activity as illustrated by (i) intrinsic fast spiking neuron abnormalities such as decreased input resistance, increased rheobase, and reduced firing rates, (ii) desynchronization or delayed temporal coupling of putative excitatory-inhibitory neuron firing, (iii) attenuation of gamma oscillations, which require fast spiking neuron firing and abate before the onset of epileptiform discharges, and (iv) unrestrained putative excitatory neuron firing congruent with fast spiking neuron hypoexcitability (49, 78). The metabolic characteristics of inhibitory neurons may account for this metabolic vulnerability. Consistent with this energy metabolism dependence of inhibition, mitochondrial dysfunction preferentially suppresses gamma oscillations (2, 26). It is possible to predict most seizures in human and mouse pyruvate dehydrogenase deficiency in advance via the measurement of gamma oscillation power, which declines minutes before seizure onset (49). We postulate the cause as depressed activity-dependent availability of TCA cycle–derived compounds such as ATP (43). This modulation may be more pronounced in inhibitory neurons, which, in addition to requiring ATP for elevated rates of basal and activity-dependent synaptic vesicular release, contain three times more K_{ATP} channels than excitatory neurons (44) and rely on ATP to promote channel closing to maintain cell membrane resistance (45). In conclusion, our present and previous results (49, 78) suggest that energy metabolism disorders preferentially impair, in fuel-modulable fashion, the activity of inhibitory neurons endowed with neural circuit stabilizing or regulatory potential.

However, the study has some limitations. EEG/fMRI studies were limited by an inability to study severely affected G1D individuals because of the need for immobility without sedation during the procedure, and these might exhibit different results. Furthermore, it is possible that seizures too brief to allow for BOLD correlation, which we did not analyze, may arise from different brain regions. ^{18}F-DG-PET results may also vary once a greater population of G1D individuals is studied. We used young adult mice, which likely exhibit different metabolic and neurophysiological activities compared to developing mice. It is also possible that investigation of additional brain regions beyond cerebral cortex and thalamus may reveal additional or complementary synaptic dysfunction mechanisms. Neurophysiological studies in brain slices are devoid of long-range inputs and likely to differ from in vivo recordings. Last, our mouse metabolic studies reflect areas of tissue rather than individual cells. Thus, it is possible that differential cellular or subcellular impacts exist in G1D.

MATERIALS AND METHODS

Study design

All experimental procedures were approved by the University of Texas Southwestern Medical Center Institutional Review Board and Institutional Animal Care and Use Committee. All G1D individuals studied harbored a pathogenic mutation in one *slc2a1* allele and were afflicted by the common G1D phenotype (6) as verified by standard clinical evaluation. Exclusion criteria for EEG/fMRI included inability to tolerate immobility under

no sedation inside the MRI scanner or metal implants precluding MRI. Human data sources included EEG, ^{18}F-FDG-PET, and EEG/ fMRI. Data sources from mice included ^{18}F-DG-PET of the entire body, histological analysis, and ^{13}C MS of brain metabolites and brain slice recordings of neuronal activity. Initial sample size calculations were based on prior data using comparable techniques (5, 18, 37). Brain slice studies were performed blinded with respect to genotype. Mouse electrocorticography (ECoG) acquisition could not be blinded because of frank ataxia in G1D mice; hence, recordings were number-coded post hoc and analyzed in a blinded fashion. For select mouse experiments, pilot data from three or four samples per group provided an estimate of SD and effect magnitude, which, together with a power of 0.8 and $P < 0.05$, guided sample sizes using the MATLAB function sampsizepwr (MathWorks Inc.). Control mice and matched G1D mice from the same litter were randomly selected for experiments, with similar male and female rations unless where stated. Replicates and statistical tests are cited with each result. Data analysis was blind and performed concurrently on control and experimental data with the same MATLAB scripts and parameters. No data, including any outlier values, were excluded. PET and MS unanalyzed data are provided in data file S1 and S2.

Statistical analysis

Prism 6.0 (GraphPad Software) was used for all statistical analyses including independent Student's *t* test assuming equal variances unless otherwise specified, paired sample t test for comparing changes in the same mouse, Mann-Whitney *U* test if the data had a nonparametric distribution, one-sample *t* test testing if the data mean was significantly different from the value of zero, and two-way ANOVA (correction for multiple comparisons controlled for false discovery rate with the method of Benjamini-Krieger-Yekutieli). The value of alpha (significance level) was set at 0.05, and all tests of significance were two-sided. All data are expressed as means ± SEM except where noted.

Supplementary Material

Refer to Web version on PubMed Central for supplementary material.

Acknowledgments:

We thank the G1D individuals who participated in the studies; J. Huguenard, E. Kavalali, and J. Gibson for electrophysiology advice; D. Nordli for assistance with EEG analysis; S. Kayani for helping medically assess the G1D individuals; and D. Veltkamp for providing three normal control PET scans.

Funding:

This work was supported by the Glut1 Deficiency Foundation (to J.M.P.) and NIH grants NS077015 (to J.M.P.), NS094257 (to J.M.P.), NS102588 (to J.M.P.), and NS116824 (to M.S.G.).

REFERENCES AND NOTES

1. Lund-Andersen H, Transport of glucose from blood to brain. Physiol. Rev 59, 305–352 (1979). [PubMed: 375257]
2. Butterworth RF, in Basic Neurochemistry: Molecular, Cellular and Medical Aspects, Brady ST, Siegel GJ, Albers RW, Price DL, Eds. (Elsevier, ed. 7, 2005).

3. Pascual JM, Campistol J, Gil-Nagel A, Epilepsy in inherited metabolic disorders. Neurologist 14, S2–S14 (2008). [PubMed: 19225367]
4. Pascual JM, Progressive Brain Disorders in Childhood (Cambridge Univ. Press, 2017).
5. Pascual JM, Van Heertum RL, Wang D, Engelstad K, De Vivo DC, Imaging the metabolic footprint of Glut1 deficiency on the brain. Ann. Neurol 52, 458–464 (2002). [PubMed: 12325075]
6. Pascual JM, Ronen GM, Glucose transporter type I deficiency (G1D) at 25 (1990-2015): Presumptions, facts, and the lives of persons with this rare disease. Pediatr. Neurol 53, 379–393 (2015). [PubMed: 26341673]
7. Siesjö BK, Brain Energy Metabolism (John Wiley & Sons, 1978).
8. Pascual JM, Liu P, Mao D, Kelly DI, Hernandez A, Sheng M, Good LB, Ma Q, Marin-Valencia I, Zhang X, Park JY, Hynan LS, Stavinoha P, Roe CR, Lu H, Triheptanoin for glucose transporter type I deficiency (G1D): Modulation of human ictogenesis, cerebral metabolic rate, and cognitive indices by a food supplement. JAMA Neurol. 71, 1255–1265 (2014). [PubMed: 25110966]
9. Hao J, Kelly DI, Su J, Pascual JM, Clinical aspects of glucose transporter type 1 deficiency: Information from a global registry. JAMA Neurol. 74, 727–732 (2017). [PubMed: 28437535]
10. Brockmann K, Wang D, Korenke CG, von Moers A, Ho YY, Pascual JM, Kuang K, Yang G, Ma L, Kranz-Eble P, Fischbarg J, Hanefeld F, de Vivo DC, Autosomal dominant glut-1 deficiency syndrome and familial epilepsy. Ann. Neurol 50, 476–485 (2001). [PubMed: 11603379]
11. Akman CI, Engelstad K, Hinton VJ, Ullner P, Koenigsberger D, Leary L, Wang D, de Vivo DC, Acute hyperglycemia produces transient improvement in glucose transporter type 1 deficiency. Ann. Neurol 67, 31–40 (2010). [PubMed: 20186957]
12. Cohen MX, Fluctuations in oscillation frequency control spike timing and coordinate neural networks. J. Neurosci 34, 8988–8998 (2014). [PubMed: 24990919]
13. Hosek RS, Sances A Jr., Jodat RW, Larson SJ, The contributions of intracerebral currents to the EEG and evoked potentials. IEEE Trans. Biomed. Eng 25, 405–413 (1978). [PubMed: 100409]
14. Epstein HT, Epstein EB, The relationship between brain weight and head circumference from birth to age 18 years. Am. J. Phys. Anthropol 48, 471–473 (1978). [PubMed: 655268]
15. Berman R, Negishi M, Vestal M, Spann M, Chung MH, Bai X, Purcaro M, Motelow JE, Danielson N, Dix-Cooper L, Enev M, Novotny EJ, Constable RT, Blumenfeld H, Simultaneous EEG, fMRI, and behavior in typical childhood absence seizures. Epilepsia 51, 2011–2022 (2010). [PubMed: 20608963]
16. Mishra AM, Bai X, Motelow JE, DeSalvo MN, Danielson N, Sanganahalli BG, Hyder F, Blumenfeld H, Increased resting functional connectivity in spike-wave epilepsy in WAG/Rij rats. Epilepsia 54, 1214–1222 (2013). [PubMed: 23815571]
17. Pascual JM, Wang D, Yang R, Shi L, Yang H, de Vivo DC, Structural signatures and membrane helix 4 in GLUT1: Inferences from human blood-brain glucose transport mutants. J. Biol. Chem 283, 16732–16742 (2008). [PubMed: 18387950]
18. Marin-Valencia I, Good LB, Ma Q, Duarte J, Bottiglieri T, Sinton CM, Heilig CW, Pascual JM, Glut1 deficiency (G1D): Epilepsy and metabolic dysfunction in a mouse model of the most common human phenotype. Neurobiol. Dis 48, 92–101 (2012). [PubMed: 22683290]
19. Deane R, Segal MB, The transport of sugars across the perfused choroid plexus of the sheep. J. Physiol 362, 245–260 (1985). [PubMed: 4020688]
20. Wu HM, Sui G, Lee CC, Prins ML, Ladno W, Lin HD, Yu AS, Phelps ME, Huang SC, In vivo quantitation of glucose metabolism in mice using small-animal PET and a microfluidic device. J. Nucl. Med 48, 837–845 (2007). [PubMed: 17475972]
21. Marin-Valencia I, Good LB, Ma Q, Jeffrey FM, Malloy CR, Pascual JM, High-resolution detection of ^{13}C multiplets from the conscious mouse brain by ex vivo NMR spectroscopy. J. Neurosci. Methods 203, 50–55 (2012). [PubMed: 21946227]
22. Vannucci SJ, Simpson IA, Developmental switch in brain nutrient transporter expression in the rat. Am. J. Physiol. Endocrinol. Metab 285, E1127–E1134 (2003). [PubMed: 14534079]
23. Wang D, Pascual JM, Yang H, Engelstad K, Mao X, Cheng J, Yoo J, Noebels JL, de Vivo DC, A mouse model for Glut-1 haploinsufficiency. Hum. Mol. Genet 15, 1169–1179 (2006). [PubMed: 16497725]

24. Tekkok SB, Godfraind JM, Krnjevic K, Moderate hypoglycemia aggravates effects of hypoxia in hippocampal slices from diabetic rats. Neuroscience 113, 11–21 (2002). [PubMed: 12123680]
25. Fogerson PM, Huguenard JR, Tapping the brakes: Cellular and synaptic mechanisms that regulate thalamic oscillations. Neuron 92, 687–704 (2016). [PubMed: 27883901]
26. Cope DW, di Giovanni G, Fyson SJ, Orbán G, Errington AC, Lőrincz ML, Gould TM, Carter DA, Crunelli V, Enhanced tonic GABAA inhibition in typical absence epilepsy. Nat. Med 15, 1392–1398 (2009). [PubMed: 19966779]
27. Jia F, Pignataro L, Schofield CM, Yue M, Harrison NL, Goldstein PA, An extrasynaptic GABAA receptor mediates tonic inhibition in thalamic VB neurons. J. Neurophysiol 94, 4491–4501 (2005). [PubMed: 16162835]
28. Richards DA, Lemos T, Whitton PS, Bowery NG, Extracellular GABA in the ventrolateral thalamus of rats exhibiting spontaneous absence epilepsy: A microdialysis study. J. Neurochem 65, 1674–1680 (1995). [PubMed: 7561864]
29. Kim U, Sanchez-Vives MV, McCormick DA, Functional dynamics of GABAergic inhibition in the thalamus. Science 278, 130–134 (1997). [PubMed: 9311919]
30. Hayar A, Shipley MT, Ennis M, Olfactory bulb external tufted cells are synchronized by multiple intraglomerular mechanisms. J. Neurosci 25, 8197–8208 (2005). [PubMed: 16148227]
31. Wada H, Okada Y, Nabetani M, Nakamura H, The effects of lactate and beta-hydroxybutyrate on the energy metabolism and neural activity of hippocampal slices from adult and immature rat. Brain Res. Dev. Brain Res 101, 1–7 (1997). [PubMed: 9263574]
32. Thio LL, Wong M, Yamada KA, Ketone bodies do not directly alter excitatory or inhibitory hippocampal synaptic transmission. Neurology 54, 325–331 (2000). [PubMed: 10668691]
33. Huguenard JR, McCormick DA, Thalamic synchrony and dynamic regulation of global forebrain oscillations. Trends Neurosci. 30, 350–356 (2007). [PubMed: 17544519]
34. Pong AW, Geary BR, Engelstad KM, Natarajan A, Yang H, de Vivo DC, Glucose transporter type I deficiency syndrome: Epilepsy phenotypes and outcomes. Epilepsia 53, 1503–1510 (2012). [PubMed: 22812641]
35. Morrisett RA, Jope RS, Snead III OC, Effects of drugs on the initiation and maintenance of status epilepticus induced by administration of pilocarpine to lithium-pretreated rats. Exp. Neurol 97, 193–200 (1987). [PubMed: 3582562]
36. Racine RJ, Modification of seizure activity by electrical stimulation. II. Motor seizure. Electroencephalogr. Clin. Neurophysiol 32, 281–294 (1972). [PubMed: 4110397]
37. Marin-Valencia I, Good LB, Ma Q, Malloy CR, Pascual JM, Heptanoate as a neural fuel: Energetic and neurotransmitter precursors in normal and glucose transporter I-deficient (G1D) brain. J. Cereb. Blood Flow Metab 33, 175–182 (2013). [PubMed: 23072752]
38. Klepper J, Florcken A, Fischbarg J, Voit T, Effects of anticonvulsants on GLUT1-mediated glucose transport in GLUT1 deficiency syndrome in vitro. Eur. J. Pediatr 162, 84–89 (2003). [PubMed: 12548383]
39. Klepper J, Fischbarg J, Vera JC, Wang D, De Vivo DC, GLUT1-deficiency: Barbiturates potentiate haploinsufficiency in vitro. Pediatr. Res 46, 677–683 (1999). [PubMed: 10590023]
40. Wong HY, Chu TS, Lai JC, Fung KP, Fok TF, Fujii T, Ho YY, Sodium valproate inhibits glucose transport and exacerbates Glut1-deficiency in vitro. J. Cell. Biochem 96, 775–785 (2005). [PubMed: 16149077]
41. Klepper J, Akman C, Armeno M, Auvin S, Cervenka M, Cross HJ, de Giorgis V, Della Marina A, Engelstad K, Heussinger N, Kossoff EH, Leen WG, Leiendecker B, Monani UR, Oguni H, Neal E, Pascual JM, Pearson TS, Pons R, Scheffer IE, Veggiotti P, Willemsen M, Zuberi SM, de Vivo DC, Glut1 deficiency syndrome (Glut1DS): State of the art in 2020 and recommendations of the international Glut1DS study group. Epilepsia Open 5, 354–365 (2020). [PubMed: 32913944]
42. Jones DM, Esmaeil N, Maren S, Macdonald RL, Characterization of pharmacoresistance to benzodiazepines in the rat Li-pilocarpine model of status epilepticus. Epilepsy Res. 50, 301–312 (2002). [PubMed: 12200221]
43. Rajasekaran K, Todorovic M, Kapur J, Calcium-permeable AMPA receptors are expressed in a rodent model of status epilepticus. Ann. Neurol 72, 91–102 (2012). [PubMed: 22829271]

44. Wang D, Pascual JM, Yang H, Engelstad K, Jhung S, Sun RP, de Vivo DC, Glut-1 deficiency syndrome: Clinical, genetic, and therapeutic aspects. Ann. Neurol 57, 111–118 (2005). [PubMed: 15622525]
45. Huntsman MM, Porcello DM, Homanics GE, DeLorey TM, Huguenard JR, Reciprocal inhibitory connections and network synchrony in the mammalian thalamus. Science 283, 541–543 (1999). [PubMed: 9915702]
46. Macdonald RL, Kang JQ, Gallagher MJ, Mutations in GABAA receptor subunits associated with genetic epilepsies. J. Physiol 588, 1861–1869 (2010). [PubMed: 20308251]
47. Brown AM, Tekkok SB, Ransom BR, Glycogen regulation and functional role in mouse white matter. J. Physiol 549, 501–512 (2003). [PubMed: 12679378]
48. Monnier LO, Owens D, Colette C, Bonnet F, Glycaemic variabilities: Key questions in pursuit of clarity. Diabetes Metab. 47, 101283 (2021). [PubMed: 34547451]
49. Jakkamsetti V, Marin-Valencia I, Ma Q, Good LB, Terrill T, Rajasekaran K, Pichumani K, Khemtong C, Hooshyar MA, Sundarrajan C, Patel MS, Bachoo RM, Malloy CR, Pascual JM, Brain metabolism modulates neuronal excitability in a mouse model of pyruvate dehydrogenase deficiency. Sci. Transl. Med 11, (2019).
50. Llinás R, Ribary U, Perception as an oneiric-like state modulated by the senses, in Large-Scale Neuronal Theories of the Brain (MIT Press, 1994), pp. 111–124.
51. Crick F, Koch C, in Seminars in the Neurosciences (Saunders Scientific Publications, 1990), vol. 2, pp. 263–275.
52. Supp GG, Siegel M, Hipp JF, Engel AK, Cortical hypersynchrony predicts breakdown of sensory processing during loss of consciousness. Curr. Biol 21, 1988–1993 (2011). [PubMed: 22100063]
53. Bartolomei F, Naccache L, The global workspace (GW) theory of consciousness and epilepsy. Behav. Neurol 24, 67–74 (2011). [PubMed: 21447900]
54. Smit H, Hacker PM, Seven misconceptions about the mereological fallacy: A compilation for the perplexed. Erkenntnis 79, 1077–1097 (2014).
55. Bennett MR, Hacker PMS, Philosophical Foundations of Neuroscience (John Wiley & Sons, ed. 2, 2022).
56. Heilig CW, Deb DK, Abdul A, Riaz H, James LR, Salameh J, Nahman NS Jr., GLUT1 regulation of the pro-sclerotic mediators of diabetic nephropathy. Am. J. Nephrol 38, 39–49 (2013). [PubMed: 23817135]
57. Allaman I, Bélanger M, Magistretti PJ, Methylglyoxal, the dark side of glycolysis. Front. Neurosci 9, 23 (2015). [PubMed: 25709564]
58. Steriade M, Llinas RR, The functional states of the thalamus and the associated neuronal interplay. Physiol. Rev 68, 649–742 (1988). [PubMed: 2839857]
59. Steriade M, Domich L, Oakson G, Reticularis thalami neurons revisited: Activity changes during shifts in states of vigilance. J. Neurosci 6, 68–81 (1986). [PubMed: 3944624]
60. Penny GR, Conley M, Schmechel DE, Diamond IT, The distribution of glutamic acid decarboxylase immunoreactivity in the diencephalon of the opossum and rabbit. J. Comp. Neurol 228, 38–56 (1984). [PubMed: 6090511]
61. Petsche H, Pockberger H, Rappelsberger P, On the search for the sources of the electroencephalogram. Neuroscience 11, 1–27 (1984). [PubMed: 6369169]
62. Meeren HK, Veening JG, Moderscheim TA, Coenen AM, van Luijtelaar G, Thalamic lesions in a genetic rat model of absence epilepsy: Dissociation between spike-wave discharges and sleep spindles. Exp. Neurol 217, 25–37 (2009). [PubMed: 19416679]
63. Douglas RJ, Martin KA, Neuronal circuits of the neocortex. Annu. Rev. Neurosci 27, 419–451 (2004). [PubMed: 15217339]
64. D'Antuono M, Inaba Y, Biagini G, D'Arcangelo G, Tancredi V, Avoli M, Synaptic hyperexcitability of deep layer neocortical cells in a genetic model of absence seizures. Genes Brain Behav. 5, 73–84 (2006).
65. Naka A, Adesnik H, Inhibitory circuits in cortical layer 5. Front. Neural Circuits 10, –35 (2016). [PubMed: 27199675]

66. Carter BC, Bean BP, Sodium entry during action potentials of mammalian neurons: Incomplete inactivation and reduced metabolic efficiency in fast-spiking neurons. Neuron 64, 898–909 (2009). [PubMed: 20064395]

67. Inan M, Zhao M, Manuszak M, Karakaya C, Rajadhyaksha AM, Pickel VM, Schwartz TH, Goldstein PA, Manfredi G, Energy deficit in parvalbumin neurons leads to circuit dysfunction, impaired sensory gating and social disability. Neurobiol. Dis 93, 35–46 (2016). [PubMed: 27105708]

68. Bal T, von Krosigk M, McCormick DA, Synaptic and membrane mechanisms underlying synchronized oscillations in the ferret lateral geniculate nucleus in vitro. J. Physiol 483 (Pt. 3), 641–663 (1995). [PubMed: 7776249]

69. Rovo Z, Matyas F, Bartho P, Slezia A, Lecci S, Pellegrini C, Astori S, David C, Hangya B, Luthi A, Acsady L, Phasic, nonsynaptic GABA-A receptor-mediated inhibition entrains thalamocortical oscillations. J. Neurosci 34, 7137–7147 (2014). [PubMed: 24849349]

70. Bright DP, Renzi M, Bartram J, McGee TP, MacKenzie G, Hosie AM, Farrant M, Brickley SG, Profound desensitization by ambient GABA limits activation of δ-containing $GABA_A$ receptors during spillover. J. Neurosci 31, 753–763 (2011). [PubMed: 21228184]

71. Zhou C, Huang Z, Ding L, Deel ME, Arain FM, Murray CR, Patel RS, Flanagan CD, Gallagher MJ, Altered cortical GABAA receptor composition, physiology, and endocytosis in a mouse model of a human genetic absence epilepsy syndrome. J. Biol. Chem 288, 21458–21472 (2013). [PubMed: 23744069]

72. Herd MB, Brown AR, Lambert JJ, Belelli D, Extrasynaptic GABA(A) receptors couple presynaptic activity to postsynaptic inhibition in the somatosensory thalamus. J. Neurosci 33, 14850–14868 (2013). [PubMed: 24027285]

73. Masur D, Shinnar S, Cnaan A, Shinnar RC, Clark P, Wang J, Weiss EF, Hirtz DG, Glauser TA; Childhood Absence Epilepsy Study Group, Pretreatment cognitive deficits and treatment effects on attention in childhood absence epilepsy. Neurology 81, 1572–1580 (2013). [PubMed: 24089388]

74. SoRelle JA, Pascual JM, Gotway G, Park JY, Assessment of interlaboratory variation in the interpretation of genomic test results in patients with epilepsy. JAMA Netw. Open 3, e203812 (2020). [PubMed: 32347949]

75. Gavrilovici C, Rho JM, Metabolic epilepsies amenable to ketogenic therapies: Indications, contraindications, and underlying mechanisms. J. Inherit. Metab. Dis 44, 42–53 (2021). [PubMed: 32654164]

76. Rangaraju V, Calloway N, Ryan TA, Activity-driven local ATP synthesis is required for synaptic function. Cell 156, 825–835 (2014). [PubMed: 24529383]

77. Zwart R, Sher E, Ping X, Jin X, Sims JR Jr., Chappell AS, Gleason SD, Hahn PJ, Gardinier K, Gernert DL, Hobbs J, Smith JL, Valli SN, Witkin JM, Perampanel, an antagonist of α-Amino-3-Hydroxy-5-Methyl-4-Isoxazolepropionic acid receptors, for the treatment of epilepsy: Studies in human epileptic brain and nonepileptic brain and in rodent models. J. Pharmacol. Exp. Ther 351, 124–133 (2014). [PubMed: 25027316]

78. Jakkamsetti V, Ma Q, Pascual JM, A subset of synaptic transmission events is coupled to acetyl coenzyme A production. J. Neurophysiol 127, 623–636 (2022). [PubMed: 35080429]

79. Evans AC; Brain Development Cooperative Group, The NIH MRI study of normal brain development. Neuroimage 30, 184–202 (2006). [PubMed: 16376577]

80. Tadel F, Baillet S, Mosher JC, Pantazis D, Leahy RM, Brainstorm: A user-friendly application for MEG/EEG analysis. Comput. Intell. Neurosci 2011, 879716 (2011). [PubMed: 21584256]

81. Ashburner J, Friston KJ, Unified segmentation. Neuroimage 26, 839–851 (2005). [PubMed: 15955494]

82. Kybic J, Clerc M, Abboud T, Faugeras O, Keriven R, Papadopoulo T, A common formalism for the integral formulations of the forward EEG problem. IEEE Trans. Med. Imaging 24, 12–28 (2005). [PubMed: 15638183]

83. Gramfort A, Papadopoulo T, Olivi E, Clerc M, OpenMEEG: Opensource software for quasistatic bioelectromagnetics. Biomed. Eng. Online 9, 45 (2010). [PubMed: 20819204]

84. Pascual-Marqui RD, Standardized low-resolution brain electromagnetic tomography (sLORETA): Technical details. Methods Find. Exp. Clin. Pharmacol 24 (Suppl. D), 5–12 (2002). [PubMed: 12575463]

85. Shattuck DW, Mirza M, Adisetiyo V, Hojatkashani C, Salamon G, Narr KL, Poldrack RA, Bilder RM, Toga AW, Construction of a 3D probabilistic atlas of human cortical structures. Neuroimage 39, 1064–1080 (2008). [PubMed: 18037310]

86. Gotman J, Kobayashi E, Bagshaw AP, Benar CG, Dubeau F, Combining EEG and fMRI: A multimodal tool for epilepsy research. J. Magn. Reson. Imaging 23, 906–920 (2006). [PubMed: 16649203]

87. Motelow JE, Blumenfeld H, Functional neuroimaging of spike-wave seizures. Methods Mol. Biol 489, 189–209 (2009). [PubMed: 18839093]

88. Sun RC, Young LEA, Bruntz RC, Markussen KH, Zhou Z, Conroy LR, Hawkinson TR, Clarke HA, Stanback AE, Macedo JKA, Emanuelle S, Brewer MK, Rondon AL, Mestas A, Sanders WC, Mahalingan KK, Tang B, Chikwana VM, Segvich DM, Contreras CJ, Allenger EJ, Brainson CF, Johnson LA, Taylor RE, Armstrong DD, Shaffer R, Waechter CJ, Kooi CWV, De Paoli-Roach AA, Roach PJ, Hurley TD, Drake RR, Gentry MS, Brain glycogen serves as a critical glucosamine cache required for protein glycosylation. Cell Metab. 33, 1404–1417.e9 (2021). [PubMed: 34043942]

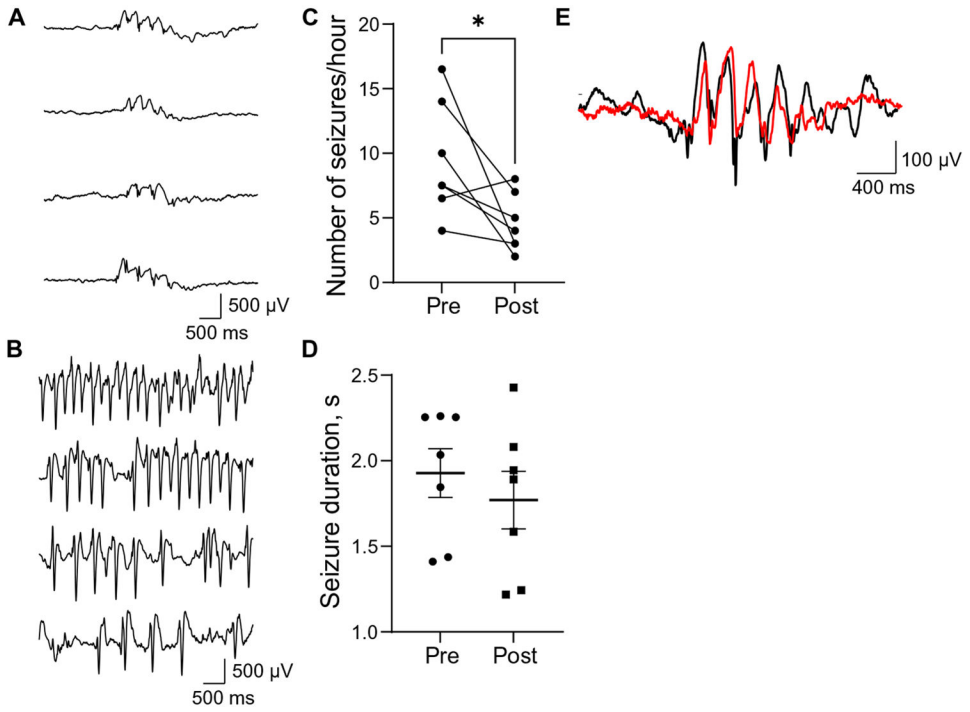

Fig. 1. Seizures, oscillation periodicity, and meal effect in G1D.

(**A**) Electroencephalographic recordings illustrating four seizures in one G1D individual at various times of the day. The seizures occurred at the following times (from top to bottom): 2:24:50 p.m., 5:31:34 p.m., 3:50:36 a.m., and 8:44:05 a.m. The oscillatory period was invariant. (**B**) Four seizures recorded from an individual with the unrelated epileptic disorder electrical status epilepticus in sleep. These seizures occurred (from top to bottom) at 12:05:49 p.m., 12:22:02 p.m., 12:22:14 p.m., and 12:05:55 p.m. and displayed spontaneously variable oscillatory frequency. (**C**) Effect of seven meals on number of seizures recorded from three G1D individuals. Pre- and post-meal comparison $*P < 0.05$, paired *t* test. (**D**) Effect (paired *t* test) of meals on seizure duration in the same individuals. Ranges, SEM. (**E**). Representative pre-meal (black trace) and post-meal (red trace) seizure in an individual from (A) illustrating similar oscillation period.

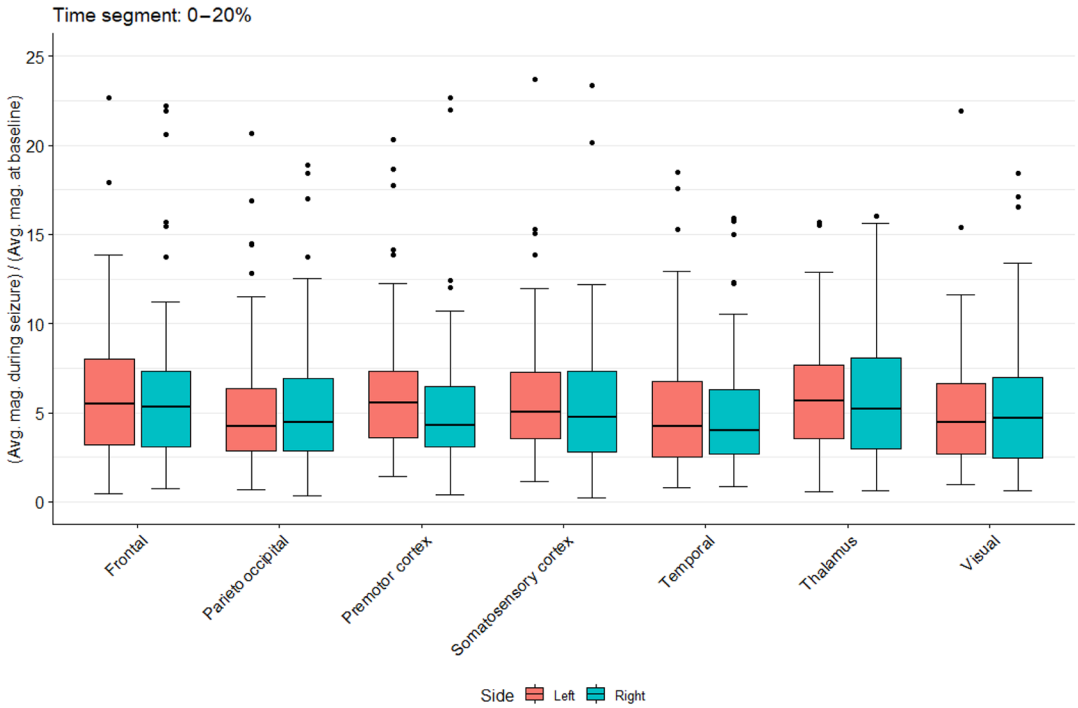

Fig. 2. EEG source localization in G1D.

Estimated current density magnitude changes relative to baseline for several modeled brain regions during the first 0 to 20% time segment of 81 seizures. Regions include several cortical areas in addition to the thalamus. The mathematical model of the brain included the cerebral ventricles and white matter as these structures influence the conduction of electricity through the brain.

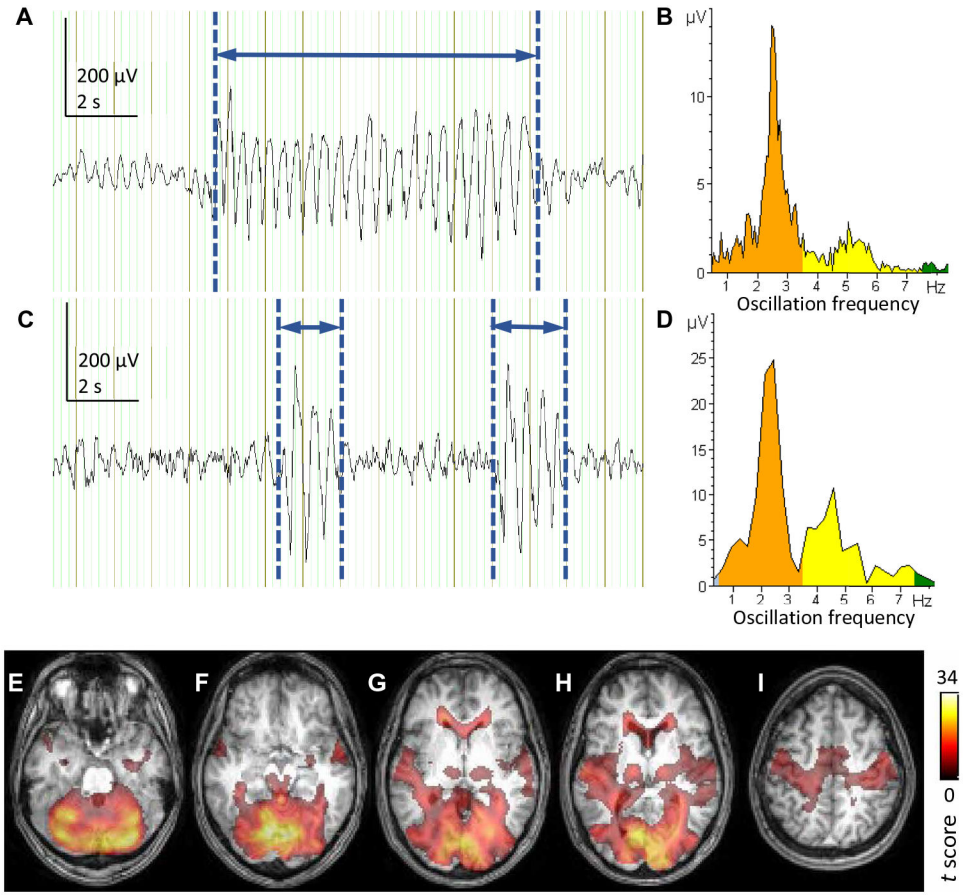

Fig. 3. Simultaneous fMRI and EEG in an individual with G1D.

(**A**). EEG trace obtained from a 22-year-old G1D individual inside a 3-T MRI scanner for correlation with the simultaneous BOLD signal after pulsation and eye blinking artifact removal. The participant was instructed to remain awake and not directed to perform tasks. In (A), one representative channel of the EEG recording is shown. A generalized seizure discharge has been manually marked using vertical blue lines, and the interval between them (horizontal blue arrow) is defined as the span of the seizure. The cumulative time span of all the seizures was divided by the total duration of the EEG recording to obtain the fraction of time that included seizures in the recording. (**B**) Frequency spectrum and electrical amplitude of the seizure oscillation in (A). (**C** and **D**) Example recording and oscillation frequency and amplitude from a 12-year-old participant for comparison with the recording and frequency analysis illustrated in (A) and (B). (**E** to **I**). BOLD fMRI signal (color) superimposed on an axial T1 weighed MRI image of the participant in (A) and (B) illustrating seizure-correlated increase in BOLD signal in the thalamus and sensorimotor cortex among other regions. The coloring of the MRI images and the rightmost scale indicate standard BOLD fMRI *t* values.

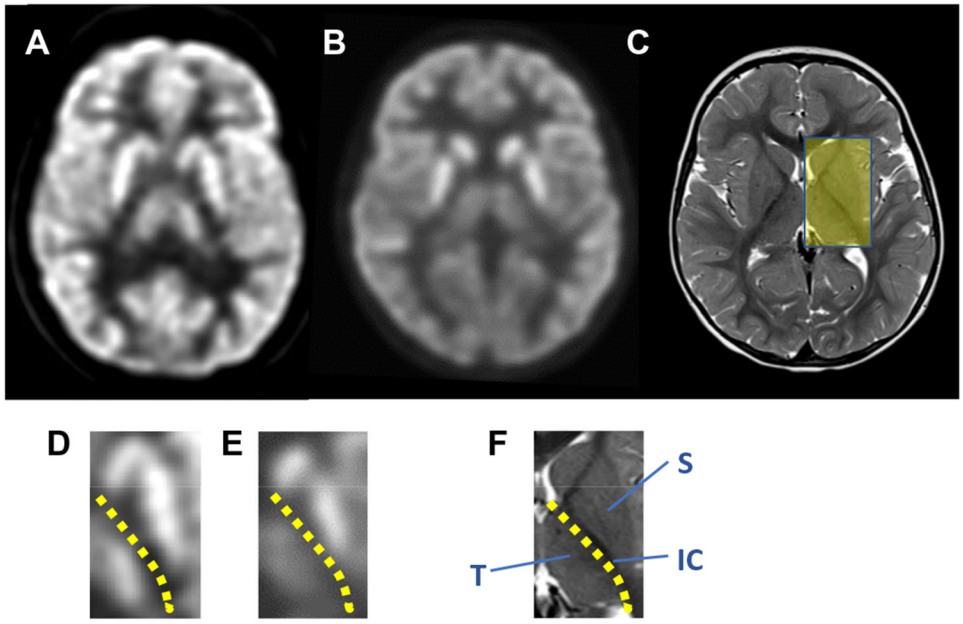

Fig. 4. ^{18}F-DG-PET in G1D.

(**A**) Axial view of an 11-year-old normal individual brain ^{18}F-DG-PET illustrating a section through the striatum and thalamus. The indication for this study was focal cortical epilepsy, which had no correlate in this normal ^{18}F-DG-PET study. (**B**) ^{18}F-DG-PET in a 7-year-old G1D individual displaying a similar sectional plane. (**C**) Axial cranial magnetic resonance image of the individual in (B) sectioned through the same approximate level. The yellow rectangle highlights the anatomical area selected for magnification in (D) to (F). (**D** to **F**). Sections through the left thalamocortical region taken from each of the images in (A) to (C), respectively. (D and E) Magnified ^{18}F-DG-PET images of the striatum (S), thalamus (T), and internal capsule (IC) from the two images displayed above (A and B). A yellow dotted line in (D), (E), and (F) demarcates the striato (S)–thalamic (T) boundary, which is occupied primarily by the internal capsule (IC).

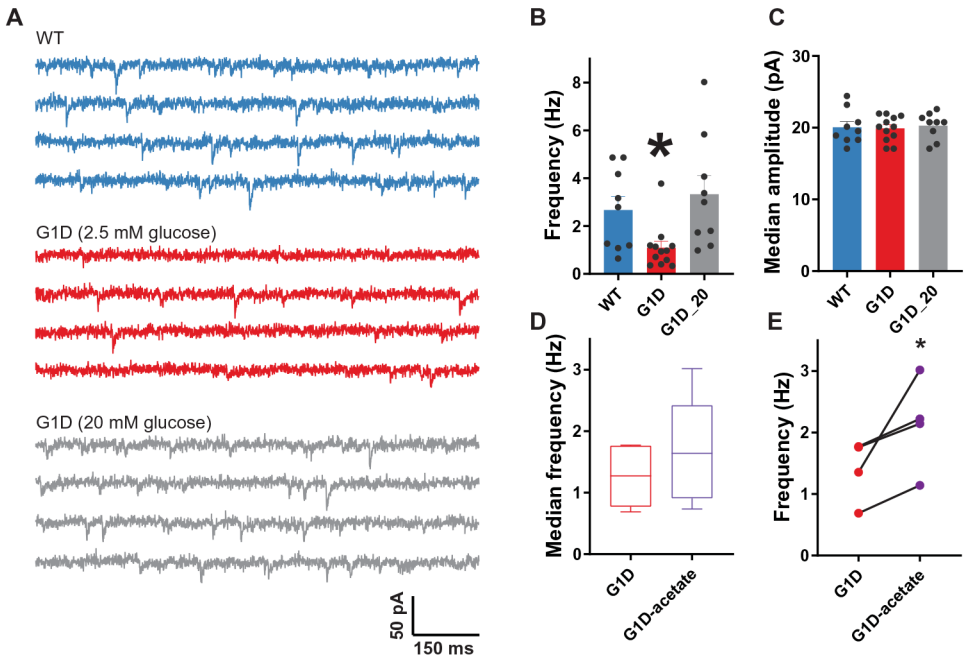

Fig. 5. Inhibitory neurotransmission onto G1D cortical pyramidal neurons.

(**A**) Representative voltage clamp recordings of mIPSCs in layer V pyramidal neurons (E_{Cl} = 0 mV) in control (WT, blue) and G1D mice perfused with 2.5 or 20 mM glucose (red and gray, respectively). (**B** and **C**) Aggregate data demonstrating differences in mean mIPSC (B) frequency and (C) amplitude in control and G1D. (**D**) Effect of replacement of 2.5 mM glucose with 5 mM acetate on median mIPSC frequency. (**E**) Paired plots of mIPSCs before and after perfusion of 5 mM acetate in G1D mice (n = 4). *P < 0.05, compared to control.

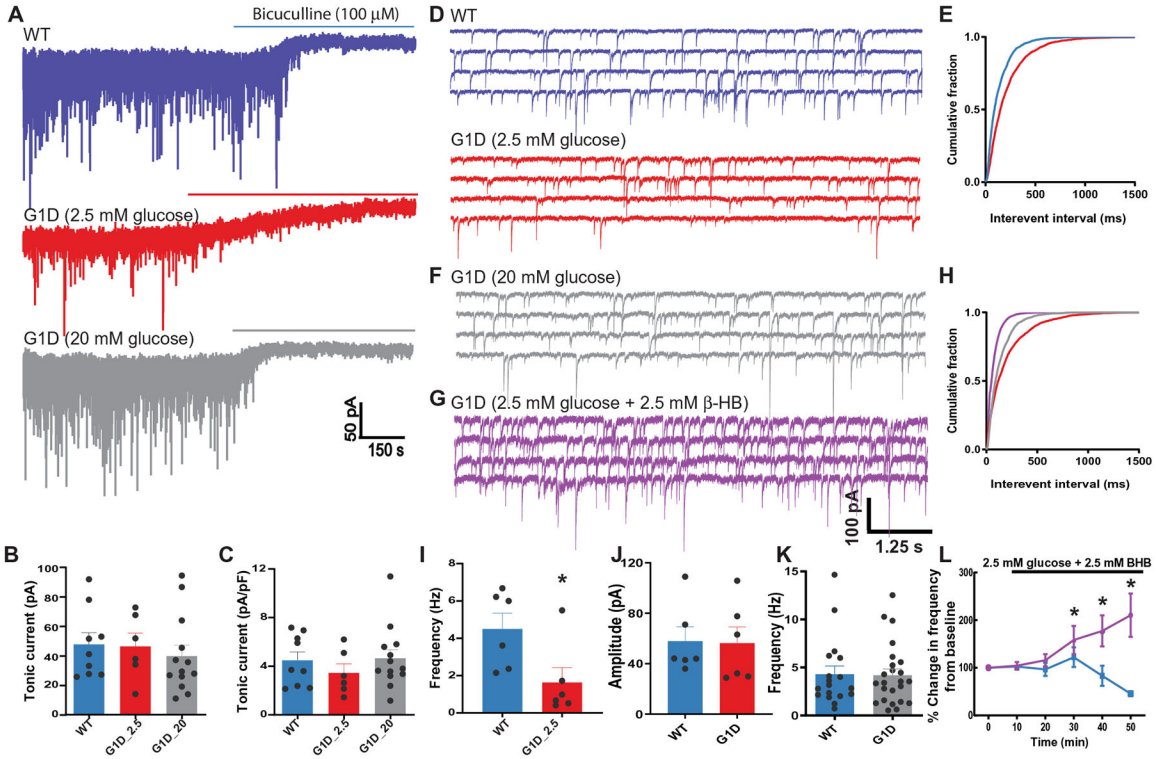

Fig. 6. Inhibitory neurotransmission onto VB relay neurons in G1D.

(**A**) Voltage clamp recordings of sIPSCs in VB relay neurons in control (WT, blue) and G1D mice (red, gray). Horizontal bar indicates the duration of perfusion of bicuculline to block both synaptic and tonic conductance. (**B** and **C**) Mean shift in holding current in recordings from control and G1D VB neurons. (**D**) Representative voltage clamp recordings as in (A) at expanded time resolution illustrating reduction in sIPSC frequency compared to control in G1D slices perfused with 2.5 mM glucose. (**E**) Cumulative probability plots of sIPSC frequency from control (blue) and G1D (red) VB relay neurons. (**F**) Voltage clamp recordings of G1D VB relay neuron perfused in 20 mM glucose shown in (A) at expanded time scale. (**G**) Voltage clamp recordings of G1D VB relay neuron perfused with 2.5 mM glucose and 2.5 mM β-HB. (**H**) Cumulative probability plots of sIPSC frequency from G1D VB relay neurons under 2.5 mM glucose (red), 20 mM glucose (gray), and 2.5 mM glucose with 2.5 mM β-HB (purple). (**I** and **J**) Summary differences in sIPSC frequency (I) and amplitude (J) between 2.5 mM glucose–perfused (red) and 20 mM glucose–perfused (blue) G1D neurons. (**K**) Summary results for sIPSC frequency on VB neurons. (**L**) Percentage change in sIPSC frequency in VB neurons (G1D, purple; control, blue) measured from recordings in 2.5 mM glucose for 10 min, followed by the addition of 2.5 mM β-HB. *$P <$ 0.05, compared to WT (I) or G1D in 2.5 mM glucose (L).

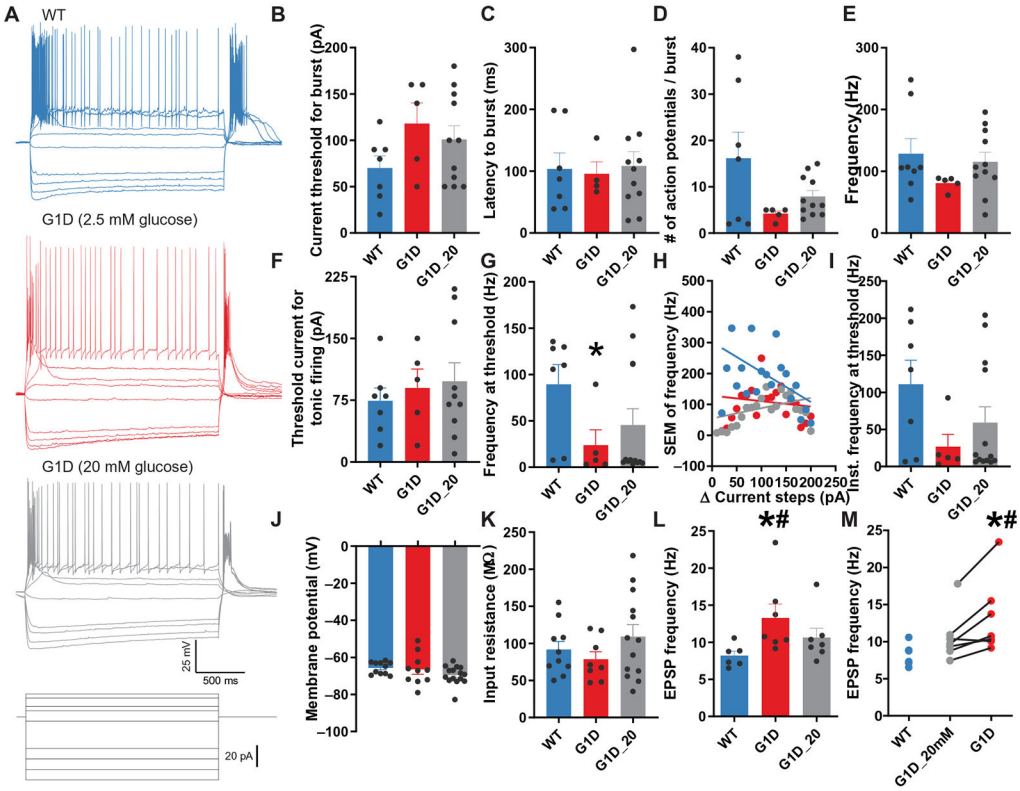

Fig. 7. Excitability of RT neurons in G1D.

(**A**) Current clamp recording from VB relay neurons of control (WT, blue), G1D in 2.5 mM glucose (red), and G1D in 20 mM glucose (gray) in response to depolarizing current steps. (**B** to **E**) Changes for the three groups illustrating burst firing properties including burst threshold current (B), burst latency (C) and number of action potentials per burst (D), and burst firing frequency (E) in G1D RT neurons perfused with 2.5 mM glucose. (**F** to **I**) Changes among the three groups illustrating tonic firing properties including tonic firing threshold current (F), action potential frequency at threshold (G), the SEM of firing frequency (H), and instantaneous action potential frequency (I). (**J** to **M**) Results from the same three groups regarding resting membrane potential (J), input resistance (K), EPSP frequency onto G1D RT neurons (L), and comparisons of EPSP frequency onto G1D RT neurons before and after perfusion with 2.5 mM glucose (M). *$P < 0.05$ compared to control; #$P < 0.05$ compared to G1D in 20 mM glucose.

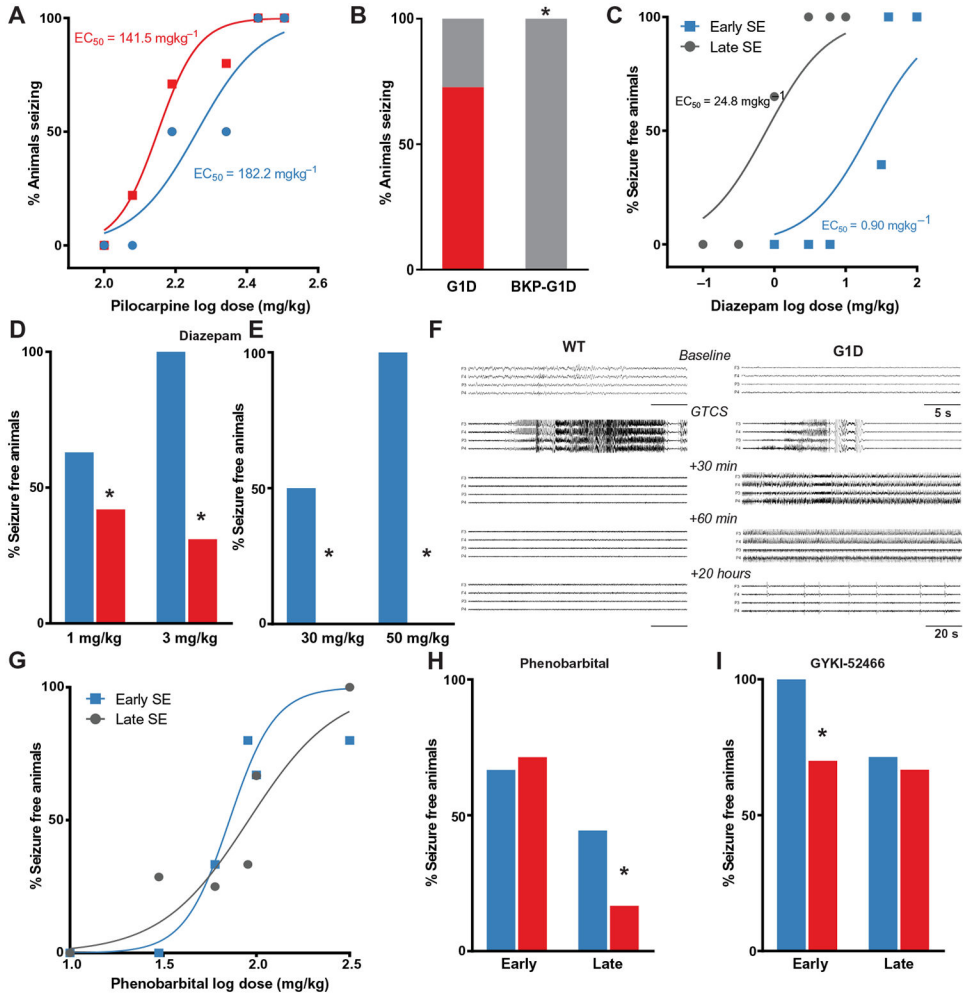

Fig. 8. Metabolic and pharmacologic treatment of G1D seizures.

(**A**) Dose-response relationship for induction of GTCS after pilocarpine administration. (**B**) Pretreatment of G1D mice with BKP effect on seizure threshold to pilocarpine-induced GTCS. (**C**) Dose-response relationship for the ability of diazepam to terminate early (blue) SE and late (black) GTCS in control mice (n = 6 to 8 mice per dose). The dose-response curve was obtained by plotting the percentage of mice that stopped seizing within 1 hour of treatment against the log dose of diazepam. ED_{50} values were obtained for early and late SE treatment groups. (**D**) Diazepam ability to terminate GTCS in control (blue) and G1D (red) mice. (**E**) Diazepam effect on GTCS termination when administered after 30 min of GTCS onset. (**F**) Representative EEG traces obtained at various times during a 24-hour period test the efficacy of diazepam administered immediately after the onset of pilocarpine-induced GTCS. (**G**) Dose-response for phenobarbital termination of GTCS in control animals. (**H**). Effect of phenobarbital on GTCS termination (**I**). Effect of the AMPA-kainate receptor antagonist GYKI-52466 on G1D mice with GTCS induced by pilocarpine, both early and late. *P < 0.05 compared to control (D, H, and I) or G1D (B).